

**PREPARATION OF NANOSIZED CeO₂
PARTICLES AND THEIR INCORPORATION
INTO TRANSPARENT ACRYLATE POLYMERS**

**A Thesis Submitted to
the Graduate School of Engineering and Sciences of
İzmir Institute of Technology
in Partial Fulfillment of the Requirements for the Degree of**

DOCTOR OF PHILOSOPHY

in Chemistry

by

Özge TUNUSOĞLU

**July 2014
İZMİR**

We approve the thesis of **Özge TUNUSOĞLU**

Examining Committee Members:

Prof. Dr. Mustafa M. DEMİR

Department of Materials Science and Engineering, İzmir Institute of Technology

Prof. Dr. Serdar ÖZÇELİK

Department of Chemistry, İzmir Institute of Technology

Prof. Dr. Muhsin ÇİFTÇİOĞLU

Department of Chemical Engineering, İzmir Institute of Technology

Assist. Prof. Dr. Yaşar AKDOĞAN

Department of Materials Science and Engineering, İzmir Institute of Technology

Assist. Prof. Dr. Aylin ZİYLAN ALBAYRAK

Department of Metallurgical and Materials Engineering, Dokuz Eylül University

21 July 2014

Prof. Dr. Mustafa M. DEMİR

Supervisor, Department of
Materials Science and Engineering,
İzmir Institute of Technology

Prof. Dr. Metin TANOĞLU

Co-supervisor, Department of
Mechanical Engineering
Izmir Institute of Technology

Prof. Dr. Ahmet Emin EROĞLU

Head of the Department of
Chemistry

Prof. Dr. R. Tuğrul SENGER

Dean of the Graduate School of
Engineering and Sciences

ACKNOWLEDGEMENTS

I would like to express my grateful thanks to my supervisor Prof. Dr. Mustafa M. DEMİR, for his instructive comments, motivations, and valued support throughout my thesis study and patience to my questions.

I am sincerely grateful to my thesis committee members Prof. Dr. Muhsin ÇİFTÇİOĞLU, Prof. Dr. Serdar ÖZÇELİK, Assist. Prof. Dr. Yaşar AKDOĞAN, and Assist. Prof. Dr. Aylin ZİYLAN ALBAYRAK for their helps and guidance for this thesis.

Special thanks to Prof Dr. Talal R.A. SHAHWAN from Birzeit University for his limitless support and belief to me. I would like to thank to Prof. Dr. Metin TANOĞLU for being co-advisor. Special thanks to Assist. Prof. Dr. Nesrin HORZUM POLAT for her supports, helps during my thesis, and for her friendship.

Special thanks to Evrim YAKUT, Gökhan ERDOĞAN and group members of Materials Research Center, Mine BAHÇECİ, Duygu OĞUZ KILIÇ, Işın ÖZÇELİK, Canan GÜNEY, and Sinem HORTOOĞLU for their helps in XRD, STEM, AFM, and TGA analysis. Also, I would like to say my special thanks to Rafael Muñoz-Espí, Ümit AKBEY, and Max Planck Institute for TEM, HRTEM, ¹³C CP-MAS, and GPC analysis. I would like to thank to Dr. Ebru KUZGUNKAYA and Dr. Hüseyin ÖZGENER for DSC and FTIR analysis.

I would like to thank to Demir Research Group and all my friends in chemistry department.

I am pleased to thank Scientific and Technological Research Council of Turkey (TUBITAK) for its financial support to this study (TBAG- (109T905)).

Finally, I would like to express my endless thanks to my mother Nurdan TUNUSOĞLU, my father Ali TUNUSOĞLU, and my sister Gözde TUNÇER, for their endless support, motivation, and patience.

ABSTRACT

PREPARATION OF NANOSIZED CeO₂ PARTICLES AND THEIR INCORPORATION INTO TRANSPARENT ACRYLATE POLYMERS

Nanoparticles having a size smaller than 100 nm are important building blocks of nanomaterials. Organically functionalized CeO₂ nanoparticles were prepared by colloidal synthesis in this work. The particles were nucleated by mixing aqueous solutions of Ce(NO₃)₃·6H₂O and ammonia at room temperature. Different small organic molecules were chosen as capping agents and injected into the reaction medium at the beginning of the synthesis: 3- (mercaptopropyl) trimethoxy silane (MPS), hexadecyltrimethyl ammonium bromide (CTAB), 3-mercapto propionic acid (3-MPA), and thioglycolic acid (TGA). The resulting nanocrystals were quasi-spherical and has a narrow mean size distribution with an average size smaller than 10 nm.

Polymerization of monomer/nanoparticle dispersion, namely in situ polymerization, has been frequently used for the fabrication of polymer nanocomposites. Both in situ and ex situ approaches were applied for surface functionalization. The particles were dispersed into methyl methacrylate and free radical polymerization was carried out. The process of nanocomposite formation was examined in terms of conversion, molecular weight, and molecular weight distribution. The polymerization responds merely to the in situ functionalized particles. Regardless of the capping agents used, the particles function as a retarder and inhibitor. Their interaction with polymerization medium shows many complexities such that molecular weight is found to be strongly dependent on the capping agent employed.

ÖZET

NANO ÖLÇEK CeO₂ TANECİKLERİNİN HAZIRLANMASI VE ŞEFFAF AKRİLİK POLİMERLER İÇERİSİNE YÜKLENMESİ

Boyutları 100 nanometrenin altında olan nanoparçacıklar, nano-malzemelerin önemli yapı taşlarıdır. Organik olarak fonksiyonelleştirilmiş CeO₂ nanoparçacıkları, kolloidal sentezle hazırlanmıştır. Parçacıklar Ce(NO₃)₃.6H₂O ve amonyak sulu çözeltilerinin oda sıcaklığında karıştırılmasıyla çekirdeklenmiştir. Kaplama maddesi olarak farklı küçük organik moleküller seçilir ve sentezin başlangıcında reaksiyon ortamına katılır: 3- (merkaptopropil) trimetoksi silan (MPS), hekzadesiltrimetill amonyum bromür (CTAB), 3-merkaptopropiyonik asit (3-MPA), and tiyoglikolik asit (TGA). Sonuçta oluşan nanokristaller yarı-küresel şekildedir ve ortalama 10 nm'den daha düşük boyut dağılımına sahiptir.

Yerinde polimerizasyon olarak adlandırılan monomer/nanoparçacık dağılımının polimerizasyonu polimer nanokompozitlerin üretiminde sıklıkla kullanılır. Yüzey fonksiyonelleştirilmesi için hem yerinde hem de doğal yeri dışında yöntemleri uygulanır. Parçacıklar metil metakrilat içinde dağıtılır ve serbest radikal polimerizasyonu uygulanır. Nanokompozit oluşumunun süreci dönüşme, moleküler ağırlık ve moleküler ağırlık dağılımı açısından incelenir. Polimerizasyon, sadece yerinde fonksiyonelleştirilen parçacıklara cevap verir. Kullanılan kaplama maddelerine bakmaksızın, parçacıklar geciktirici ve inhibitör olarak fonksiyon göstermektedir. Parçacıkların polimerizasyon ortamıyla etkileşimi birçok karmaşıklık gösterir öyle ki, molekül ağırlığının uygulanan kaplama maddesine güçlü bir şekilde bağlı olduğu bulunmuştur.

Dedicated to my family...

TABLE OF CONTENTS

LIST OF FIGURES.....	ix
LIST OF TABLES.....	xii
CHAPTER 1. INTRODUCTION.....	1
CHAPTER 2. FORMATION OF SURFACTANT-ASSISTED CeO ₂ NANOPARTICLES.....	6
2.1. Experimental	6
2.1.1. Materials and Methods	6
2.1.2. Characterization.....	9
2.2. Results and Discussion.....	10
2.2.1. Optimization of CeO ₂ Nanoparticle Synthesis.....	10
2.2.1.1. Effect of Synthesis Method	10
2.2.1.2. Effect of Reactant	22
2.2.1.3. Effect of Reactant Ratio	23
2.2.1.4. Effect of Reaction Temperature	24
2.2.1.5. Effect of Direct and Reverse Strike	24
2.2.2. Characterization of CeO ₂ Nanoparticle	25
2.2.3. Surface Chemistry and Stability of Particle Dispersion	30
2.2.4. The Mechanism of Particle Formation	41
CHAPTER 3. EFFECT OF SURFACE FUNCTIONALIZED CeO ₂ NANOPARTICLES IN FREE RADICAL BULK POLYMERIZATION OF METHYL METHACRYLATE.....	44
3.1. Experimental	44
3.1.1. Materials and Methods	44
3.1.2. Characterization	44
3.2. Results and Discussion	45
3.2.1. In-situ Polymerization of CeO ₂ /MMA Dispersion	45
3.2.2. Conversion	45

3.2.3. Molecular Weight and Molecular Weight Distributions (MWD).....	48
3.2.3.1. Capping Agents Only without the Ceria Particles	49
3.2.3.2. Unfunctionalized Particles	51
3.2.3.3. In situ Functionalized Particles	52
3.2.3.4. Ex situ Functionalized Particles	54
3.2.4. Level of Nanoparticle Dispersion in PMMA	55
3.2.5. Thermal Properties of Nanocomposites	56
 CHAPTER 4. CONCLUSIONS AND RECOMMENDATIONS.....	 62
 REFERENCES.....	 64

LIST OF FIGURES

<u>Figure</u>	<u>Page</u>
Figure 2.1. Chemical structures of surfactants.....	8
Figure 2.2. Synthesis of CeO ₂ nanoparticles showing in situ and ex situ surface functionalization step-by-step	9
Figure 2.3. Characterization of CeO ₂ particles obtained by hydrothermal synthesis (a) XRD diffractrogram and (b) particle size distribution in monomer matrix	11
Figure 2.4. Characterization of CeO ₂ particles obtained by chemical precipitation (a) XRD diffractrogram and (b) particle size distribution in monomer matrix	11
Figure 2.5. UV-VIS spectra of (a) CeO ₂ synthesized by addition of CTAB, (b) CeO ₂ and (c) CeO ₂ synthesized by addition of TGA at room temperature and atmospheric pressure with HMTA as a precursor	13
Figure 2.6. Particle size of CeO ₂ nanoparticles synthesized by HMTA with respect to time (min) estimated from UV-VIS spectra. ■ unfunctionalized ceria, CeO ₂ synthesized by addition of ● CTAB, ▲ 3MPA, ▼ TGA, and ◀ MPS.....	15
Figure 2.7. XRD pattern of CeO ₂ particles synthesized by HMTA: unfunctionalized and functionalized particles in presence of MPS, CTAB, 3MPA, and TGA	15
Figure 2.8. X-ray diffraction patterns of AOT-coated cerium oxide nanoparticles (top), bulk CeO ₂ (middle) and bulk Ce ₂ O ₃ (bottom) (Z Wu et al., 2001)....	16
Figure 2.9. TEM images of CeO ₂ particles synthesized by HMTA (a) unfunctionalized, and (b) functionalized by CTAB	17
Figure 2.10. FTIR spectra of CeO ₂ particles synthesized by HMTA: unfunctionalized and functionalized in presence of MPS, CTAB, 3MPA, and TGA	18
Figure 2.11. Fluorescence spectra of CeO ₂ particles synthesized by HMTA (a) unfunctionalized, and functionalized in the presence of (b) MPS, (c) CTAB, (d) 3MPA, and (e) TGA	19

Figure 2.12. TGA curves of CeO ₂ particles synthesized by HMTA (a) unfunctionalized and functionalized in the presence of (b) MPS, (c) CTAB, (d) 3MPA, and (e) TGA	20
Figure 2.13. Particle size distribution of CeO ₂ nanoparticle synthesized by HMTA (dispersed in methyl methacrylate) ■ unfunctionalized, functionalized by ● MPS, ▲ CTAB, ▼ TGA.....	21
Figure 2.14. XRD pattern of CeO ₂ particles synthesized by reacting reagent couples (a) cerium acetate-ammonium hydroxide, (b) cerium nitrate hexahydrate-hexamethylene tetraamine, and (c) cerium nitrate hexahydrate-ammoniumhydroxide.....	22
Figure 2.15. pH change of both unfunctionalized and functionalized CeO ₂ nanoparticles during synthesis.....	24
Figure 2.16. XRD pattern of CeO ₂ particles synthesized by NH ₄ OH (a) in situ and (b) ex situ synthesized	25
Figure 2.17. Structural models of (a, b) in situ and ex situ functionalized particles and TEM micrographs of in situ and ex situ (c, d) MPS, (e, f) CTAB, (g, h) MPA, and (i, j) TGA functionalized CeO ₂ nanoparticles synthesized by NH ₄ OH.....	27
Figure 2.18. High resolution TEM micrographs of CeO ₂ particles synthesized by NH ₄ OH: (a) unfunctionalized and in-situ functionalized by (b) CTAB, (c) MPS	29
Figure 2.19. FTIR spectra of CeO ₂ particles as-synthesized by NH ₄ OH (a) in situ functionalized and (b) ex situ functionalized	30
Figure 2.20. ¹³ C CP-MAS spectrum of CeO ₂ particles synthesized by NH ₄ OH: in situ surface functionalized in the presence of (a) MPS, and (b) 3MPA	33
Figure 2.21. Fluorescence spectra of CeO ₂ nanoparticles in situ synthesized by NH ₄ OH	34
Figure 2.22. Mass loss curves of the CeO ₂ particles as-synthesized by NH ₄ OH (a) in situ functionalized and (b) ex situ functionalized	35
Figure 2.23. Thermogram of in situ and ex situ CTAB-capped ceria particles	36
Figure 2.24. Zeta potentials of CeO ₂ particles synthesized by NH ₄ OH: in situ unfunctionalized and functionalized particles in presence of MPS, CTAB, and TGA dependent on pH values	37

Figure 2.25. Particle size distributions of unfunctionalized and functionalized CeO ₂ nanoparticles synthesized by (a) in situ and (b) ex situ method	38
Figure 3.1. Conversion of MMA in presence of in situ functionalized CeO ₂ nanoparticles at 80 °C	46
Figure 3.2. Conversion of MMA in the presence of (a) in situ and (b) ex situ functionalized CeO ₂ nanoparticles at 60 °C	47
Figure 3.3. Molecular weight distribution of PMMA in presence of (a) cerium oxide functionalized in situ, (b) capping agents, and (c) ex situ over 1020 min of polymerization at 60 °C	48
Figure 3.4. The reaction mechanism between CTAB and BPO	50
Figure 3.5. FTIR spectra of (a) unfunctionalized CeO ₂ , (b) BPO, and (c) CeO ₂ -BPO particles	52
Figure 3.6. AFM images of in situ (a) and ex situ (b) TGA functionalized CeO ₂ nanoparticles.....	55
Figure 3.7. (a) TGA demonstration of neat PMMA and its composites and (b) DTG curves of thermal decomposition of neat PMMA and its composites prepared by both unfunctionalized and functionalized CeO ₂ nanoparticles at 60 °C.....	58
Figure 3.8. Glass transition temperature (T _g / °C) of PMMA in presence of (a) capping agents, and cerium oxide functionalized in situ (b) and ex situ (c) at 60 °C	59

LIST OF TABLES

<u>Table</u>	<u>Page</u>
Table 2.1. Particle size and crystallite size values of each synthesized ceria nanoparticles by HMTA under ambient pressure and at room temperature. The particle size was estimated using Eq (2.1) at 1 hour and the size of crystals was obtained at 3 hours from XRD pattern by Debye-Scherrer.....	17
Table 2.2. Percent yield values of CeO ₂ obtained by reacting various reagents.....	23
Table 2.3. Crystallite values of the ceria nanoparticles synthesized by NH ₄ OH under ambient pressure and at room temperature. The size of crystals was obtained from XRD pattern by using Scherrer's equation taking into account (111) reflection.....	26
Table 2.4. Crystallite values of synthesized ceria nanoparticles obtained by TEM micrographs	26
Table 2.5. Vibrational band shifts and full width half maximum (FWHM) values of FTIR bands	32
Table 2.6. Mean diameter values of both in situ and ex situ synthesized particles obtained from DLS in MMA	39
Table 2.7. Graft density estimated by thermogravimetric analysis and particle size	40
Table 2.8. Comparison of the intensity ratio of (111) and (200) reflections in XRD patterns.....	42
Table 3.1. Number molecular weight (M _n) and polydispersity index (PDI) of PMMA in the presence of neat capping agents, and cerium oxide functionalized in situ and ex situ over 1020 min of polymerization at 60 °C	49
Table 3.2. Particle domain size in PMMA based on the statistical treatment of particles domains in tapping mode AFM phase images	55
Table 3.3. Glass transition temperatures (T _g /°C) of PMMA prepared in the presence of capping agents, ceria nanoparticles surface functionalized both in situ and ex situ approaches at 60 °C.....	60

CHAPTER 1

INTRODUCTION

Rare-earth metal oxides arise great interest in materials science, because the presence of 4f electrons results in attractive optical, magnetic, and chemical properties (Taguchi et al. 2009). Ceria (CeO_2) is one of the most frequently studied rare earth metal oxides and possesses unique physicochemical properties, such as absorption of ultraviolet radiation (Corma et al. 2004), gas sensing (Maskell 2000), and catalytic properties (Larese et al. 2006, Lu et al. 2009). Moreover, it is a wide band gap semiconductor, with a band gap of 3.2 eV (Orel and Orel 1994). Most of the advanced applications of CeO_2 generally appear in the nanosized regime, in which many physical properties are strongly size dependent and show significant quantum size effects. Many new potential applications for nanometric ceria—including solar cells, nanolasers, and other highly functional and effective devices—are under current discussion (Lin and Chowdhury 2010). The synthesis of nanosized ceria particles have been achieved by many different methods. Supercritical hydrothermal (Taguchi et al. 2009), conventional hydrothermal (Masui et al. 2003), solvothermal (Kepenekci et al. 2011), and pyrolytic (Oh and Kim 2007) syntheses are the four major methods to fabricate nanosized powder. The synthesis methods require hard conditions at extreme temperature and pressure; they are also still limited in the amount of nanoparticles. However, chemical precipitation provides a promising pathway for large scale production of nanosized particles at ambient conditions (Zhang et al. 2002, Palard et al. 2010, Zhou et al. 2002). Polymer/nanoparticle composites with tunable composition and morphology often exhibit multiple functionalities and even novel properties (Demir et al. 2009), which may lead to applications in diverse areas such as optoelectronics. The performance of composite materials strongly depends on the homogeneity of the particle dispersion. The control of the surface chemistry of particles is a key point to obtain well-defined and homogeneous dispersions of host particles in guest polymer matrices. Post-synthetic modification has usually been employed to introduce desired functionalities onto the surface of nanoparticles. Nanoparticles are typically treated with surfactant molecules in dispersion. This treatment modifies the surface chemistry of particle domains, which are

generally formed by pseudo-aggregates of a group of particles. Thus, the surface cannot be functionalized evenly and the particle dispersion is negatively affected. The precipitation in the presence of surfactant molecules (i.e., controlled precipitation) is an efficient approach to obtain homogeneous surface modification of the particles in one step and it allows the size and the surface chemistry to be controlled (Demir et al. 2006). The use of a minute amount of a surface-active reagent—which could be a small molecule or a macromolecule—in the reaction mixture has been considered a powerful pathway to prepare nanoparticles with a desired surface chemistry (Demir et al. 2007, Muñoz-Espí et al. 2006). Recently, Taniguchi et al. reported the synthesis of organophilic CeO₂ nanoparticles by a single step reaction of a cerium oleate complex with NH₄OH (Taniguchi et al. 2008). The reaction was carried out at room temperature in an aqueous medium. The authors claimed that the oleate links to the surface of CeO₂ particles by chemical bonding and render the particles surface an organophilic nature. The same research group performed supercritical hydrothermal synthesis of hydrophilic polymer-modified CeO₂ nanoparticles. Water-soluble polymers (e.g., polyvinyl alcohol or polyacrylic acid) were employed in the reaction mixture as surface modifiers. As a result, 20 nm cuboctahedral water-dispersible CeO₂ nanoparticles were obtained (Taguchi et al. 2011). Using a similar strategy, Yu et al. synthesized high quality CeO₂ nanocrystals by stabilization with the double hydrophilic block copolymer poly(ethylene glycol)-block-poly(methacrylic acid) as a stabilizer (Yu et al. 2004). Monodisperse CeO₂ particles with less than 2 nm diameter were synthesized by hydrothermal hydrolysis at 120 °C.

In the present work, we report a novel and very versatile synthesis of surface-functionalized CeO₂ nanocrystals by chemical precipitation at room temperature in aqueous solutions containing various capping agents. Nanoparticles with a variety of surface chemistry can be prepared. Four small surfactant molecules were used: 3-(mercaptopropyl) trimethoxy silane (MPS), hexadecyltrimethyl ammonium bromide (CTAB), 3-mercaptopropionic acid (3-MPA), and thioglycolic acid (TGA). The dispersibility of the produced particle domains were investigated in a hydrophobic monomer, methyl methacrylate, by determining the particle size distribution by DLS.

Composites of polymer matrices and nanoscale inorganic building blocks have shown the development of new or at least improved material properties such as high/low refractive index (Lin et al. 2010), thermal stability (Demir et al. 2007), toughness (Tjong 2006), high yield strength (LeBaron et al. 1999), high conductivity

(Moniruzzaman and Winey 2006), gas and solvent transport (Gorassi et al. 2003, Nazarenko et al. 2007), wear and scratch resistance (Ahmadi et al. 2007, Olad and Rasouli 2010, Wang et al. 2008), etc. Interfacial attraction has been recognized as an important parameter for composite materials. It determines the processability, microstructure, and accordingly the macroscopic properties of the resulting material (Demir and Wegner 2012). This is because fundamental understanding of polymer–inorganic interface is a critical challenge in polymer nanocomposites.

In situ polymerization has attracted considerable attention for the preparation of homogeneous nanocomposites (Demir and Wegner 2012). It involves dispersion of particles into a monomer or monomer formulation, and then subsequent polymerization is carried out in the presence of the nanoparticles. Mixing polymer chains and nanosized particles at the molecular level, which is in fact the ultimate goal for polymer nanocomposites, can be readily achieved when this process is employed. In conjunction with this advantage, it has been shown that the composites prepared by in situ polymerization offer materials with better physical properties compared to the composite prepared by simple blending, although identical material components are used at identical composition. Recent examples could be PMMA/ZnO for thermal stability (Anzlovar et al. 2010, Zhang et al. 2011), polyimide/multi walled carbon nanotubes for high conductivity (Wu et al. 2012), poly(p-phenylene benzobisoxazole)/multi walled carbon nanotubes for UV–vis absorption (Zhou et al. 2012), and polypropylene/clay (Baniasadi et al. 2010) for better mechanical properties. The reason for the improvements in material properties has been usually attributed to homogeneous internal structure. Besides, we think that the improvements may also be a consequence of interfacial attraction between particle surface and propagating polymer chain. Considering that polymer chains are initiated and grow in the presence of nanoparticles, an interaction with the particle surface and reactive propagating chain is highly possible. For instance, our group previously proposed that hydroxyl groups available on the ZnO surface may induce a degenerative transfer in free radical polymerization of MMA initiated by 2,2'-azobis(isobutyronitrile) (AIBN) (Demir et al. 2007, Demir et al. 2006). It is claimed that this interaction suppresses the formation of chains having vinylidene end groups and head-to-head links. Thermal stability of the composite material, as a result, is remarkably improved compared to the same composites prepared by blending. The interaction of propagating radicals with surface hydroxyl groups suppresses the undesirable gel effect, which leads to a better control over both the heat evolution

during the late stages of polymerization and the molecular weight distribution. The improvement in both thermal properties and the polymerization process of PMMA/ZnO was seen as a consequence of the interaction of surface hydroxyl groups and growing polymer chains.

According to the best of our knowledge, there is no clear picture about the effect of other functional groups such as $-\text{COOH}$, $-\text{SH}$, $-\text{OCH}_3$, and aliphatic chains on the in situ polymerization process. Therefore, it is important to understand the effect of nanoparticles functionalized with these chemical groups on the process of in situ polymerization. In this work, organophilic ceria nanoparticles were prepared using various capping agents 3-(mercaptopropyl) trimethoxy silane (MPS), hexadecyltrimethyl ammonium bromide (CTAB), 3- mercapto propionic acid (3-MPA), and thioglycolic acid (TGA) such that the surface of particles is varied with different functional groups. Both in situ and ex situ approaches were employed for surface functionalization. The surface-functionalized particles either in situ or ex situ are referenced as ceria(-capping agent), e.g., ceria(-CTAB), throughout the text. The particles were dispersed into bulk MMA and the effect of particle surface on the process of in situ bulk polymerization was studied. MMA is a frequently used monomer in industry for the production of commercial organic glass (Hess et al. 2009). It has been commonly polymerized by the free radical mechanism, which is well studied in the literature (Campos et al. 2005). Furthermore, ceria is a substrate on which various functional groups can be chemically grafted (Parlak and Demir 2011). It has unique physical properties such as high refractive index (Lin et al. 2010), absorbance over UVA region (Corma et al. 2004), and high catalytic activity for water gas shift reaction (Lawrence et al. 2011), fuel cells (Lee and Bowman 2006, Stevens 1999), and oxidation (Murray et al. 1999). The combination of MMA and ceria can be a good model system to study the reactivity of particle surface on free radical polymerization in nanocomposite formation.

Bulk polymerization was carried out since it allows rapid process with high conversion, high purity, and ease of handling (Saric et al. 2006). Conversion and molecular weight (MW) were examined by gravimetry and gel permeation chromatography (GPC), respectively. Thermal decomposition was determined by thermogravimetric analysis (TGA) and glass transition temperature (T_g) of the composites was measured by differential scanning calorimeter (DSC). Through these approaches we attempt to identify the interactions of surface functionality with

propagating PMMA radicals. Polymerizations of neat MMA, MMA in the presence of mere capping agents, and MMA in the presence of unfunctionalized ceria nanoparticles were studied as control systems. The overall results suggest that polymerization is retarded in the presence of the in situ functionalized particles, independent of the chemistry of the capping agents. Moreover, MW and MWD were found to strongly depend on the chemistry of capping agent.

CHAPTER 2

FORMATION OF SURFACTANT-ASSISTED CeO₂ NANOPARTICLES

2.1. Experimental

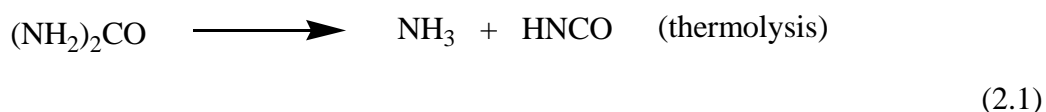
2.1.1. Materials and Methods

There are various reported synthesis methods for the production of nanoparticles. The aim in the synthesis is to control the size and size distribution, crystallinity, and shape of nanoparticles. Therefore, three of the various techniques were selected for the synthesis of CeO₂ nanoparticles: hydrothermal synthesis, chemical precipitation, and colloidal synthesis.

In hydrothermal synthesis, cerium oxide particles were prepared at room temperature and atmospheric pressure. First of all, 0.5 g of Ce(NO₃)₃·6H₂O was dissolved in 3 ml of distilled water in a beaker. Then, 1.25 g CTAB and 15 ml of 2.5 M of NaOH were added to the same beaker, respectively. The slurry was poured to the autoclave under atmospheric pressure and placed in the oven which was adjusted to 180 °C beforehand. After six hours, the autoclave was taken from oven and the slurry was filtered. The precipitate was washed by both ethanol and distilled water. Then, the solid particles were dried at 80 °C in an oven for 48 hours.

In chemical precipitation, cerium oxide nanoparticles were synthesized by setting up a reflux system. 1.5 M Ce(NO₃)₃·6H₂O and 0.5 M urea (CO(NH₂)₂) were prepared by dissolving these reagents in DMF ((CH₃)₂COHN). Then 12.5 ml each reagent was taken for the experiment. The temperature of the oil bath of reflux system was adjusted to 120 °C and 1.5 M Ce(NO₃)₃·6H₂O was poured to the balloon and attached to the system. After that, the second reagent urea was also placed in the oil bath. When the thermal equilibrium was established, urea was added to 1.5 M Ce(NO₃)₃·6H₂O dropwise. The first color change from colorless to pale yellow was observed within 45 minutes. The reflux system was operated for 6 hours. Then, the

slurry was taken to falcon tube in order to separate the solid part from the liquid part by centrifugation. After one hour centrifugation in 6000 rpm, the solid particles were washed by ethanol and dried at 45 °C under 0.5 atm vacuum overnight. For surface functionalization, each capping agent was added to the reflux system as soon as urea was added to the system without making pH control. The rest of the experiment process was the same with the unfunctionalized particle synthesis. The decomposition reaction of urea is given in Equation (2.1).



In colloidal synthesis, cerium oxide particles were synthesized at room temperature by reacting 0.5 M of cerium nitrate hexahydrate, $\text{Ce}(\text{NO}_3)_3 \cdot 6\text{H}_2\text{O}$ (Merck-extra pure) and 1.5 M hexamethylenetetraamine, $(\text{CH}_2)_6\text{N}_4$ (Sigma-Aldrich 99+%). All reagents were used without any further purification. The nanoparticles obtained were separated from mixture by centrifugation at a rate of 6000 rpm for 2 hours. The product was dried at atmospheric pressure after washing with deionized water (Zhang et al. 2004). For surface functionalization, each surfactant was added to the mixture at the first minute of reaction, separately and the same experimental process was performed. For surface functionalization, the precipitation was repeated in presence of various surfactants involving different functional group: 3-(mercaptopropyl) trimethoxy silane (MPS, Aldrich, 95%), hexadecyltrimethyl ammonium bromide (CTAB, Aldrich), 3-mercaptopropionic acid (MPA, Alfa Aesar), and thioglycolic acid (TGA, Merck). All reagents were used without any further purification. The structure of each surfactant is given in Figure 2.1.

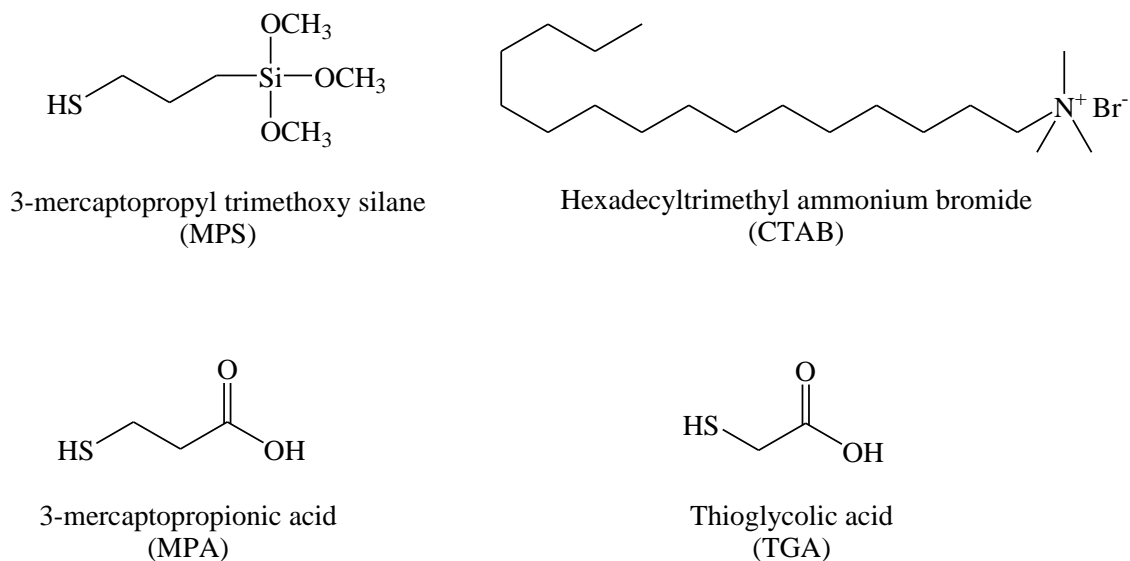
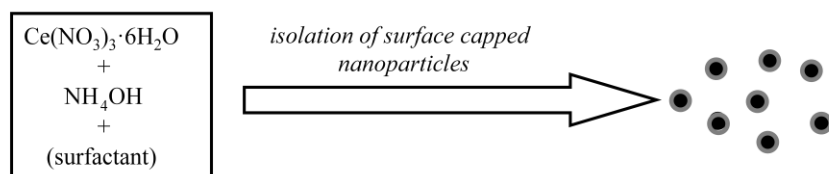


Figure 2.1. Chemical structures of surfactants

In order to obtain high yield of nanometer sized particles, colloidal CeO_2 nanoparticles were synthesized by reacting 10 ml of 0.05 M $\text{Ce}(\text{NO}_3)_3 \cdot 6\text{H}_2\text{O}$ (Merck, extra pure solution) and 10 ml of 0.5 M NH_4OH (Merck) aqueous solutions for 3 hours at 22 °C and under atmospheric pressure. Unfunctionalized nanoparticles were separated by centrifugation at 6000 rpm for 1 h. Then, collected nanoparticles were washed with both deionized water and ethanol twice. Finally, the product was dried in a vacuum oven overnight at 45 °C. For surface functionalization, the precipitation was repeated in presence of various surfactants involving different functional group.

Surface functionalization was provided by performing two methods: in situ and ex situ. In in situ surface functionalization, 2.65×10^{-5} mol of each surfactant was added to the mixture at the first minute of reaction. The same process was applied for isolation of nanoparticles. For ex-situ functionalized CeO_2 particles, the synthesis was performed in two steps. First, unfunctionalized particles were obtained by precipitation of 40 ml 0.05 M $\text{Ce}(\text{NO}_3)_3 \cdot 6\text{H}_2\text{O}$ and 40 ml 0.5 M NH_4OH and the particles were dispersed into 50 ml ethanol. Then, the alcoholic dispersion was sonicated in ultrasonic bath in order to achieve better dispersion. For a second step, the desired capping agent was added into the particle dispersion and they were allowed for surface functionalization for 12 h. Finally, the particles were obtained by centrifugation and dried under vacuum. The cartoon demonstration of preparation of nanoparticles is given in Figure 2.2.

in situ surface modification:



ex situ surface modification:

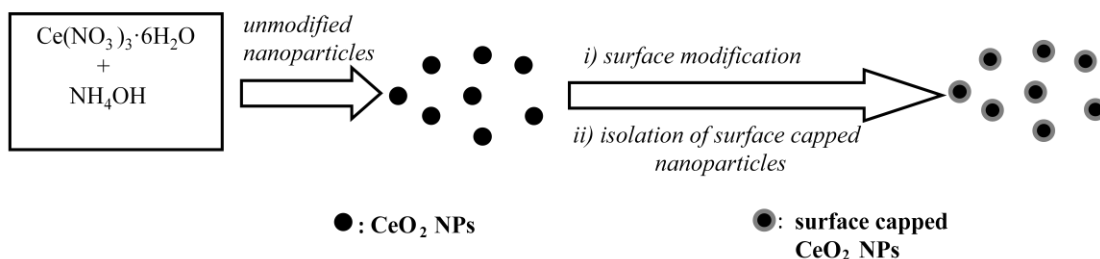


Figure 2.2. Synthesis of CeO_2 nanoparticles showing in situ and ex situ surface functionalization step-by-step.

2.1.2. Characterization

Transmission electron microscopy (TEM) was performed in a Zeiss EM 902 microscope operated at 80 kV. High-resolution TEM micrographs were taken by FEI Technai F20 microscoper performed at 200 kV. The phase structure of synthesized particles were characterized by X-ray diffraction (XRD, Philips X'pert Pro) with a Cu $K\alpha$ radiation source ($\lambda = 1.54 \text{ \AA}$). Scherrer's equation was applied in order to determine average size of crystallites

$$t = \frac{0.9 \lambda}{B \cos \theta} \quad (2.2)$$

where t is the diameter of the particle, λ is the wavelength of Cu $K\alpha$ radiation, B is the line broadening (full width half maximum), and θ is the angle of the peak center (2.2). Fourier transform infrared (FTIR) spectra were recorded by using Perkin Elmer Spectrum 100 instrument operating in the $4000\text{-}400 \text{ cm}^{-1}$ wavenumber range with resolution of 4 cm^{-1} and 20 scans. Thermogravimetric analysis was performed by Mettler Toledo ThermoSTAR TGA/SDTA 851 thermobalance by heating from room

temperature to 1000 °C at a heating rate of 10 °C min⁻¹ under nitrogen gas. The size distributions of particles in monomer methyl methacrylate (Fluka) were examined by Malvern Zetasizer Nano-ZS Nano Series dynamic light scattering instrument where the viscosity and the refractive index of the medium are selected as 0.584 mPa s and 1.414 at 20 °C, respectively. Photoluminescence emission spectra of dispersions in methyl methacrylate were investigated in a Varian Cary Eclipse Fluorescence spectrophotometer by exciting at 250 nm and monitoring the emission between 300 and 450 nm. ¹³C cross-polarization (CP) magic-angle spinning (MAS) nuclear magnetic resonance (NMR) spectra were collected by a Bruker Avance spectrometer operating at 100.6 MHz ¹³C Larmor frequency. All CP-MAS spectra have been recorded with 1 s recycle delay, 2 ms CP contact time, 100 kHz RF nutation frequency for proton and carbon (2.5 μs for 90° pulse length), at ~9 kHz MAS frequency, and by utilizing the TPPM scheme for proton decoupling. 50 and ~59 kHz spin lock pulses were applied for the cross-polarization transfer.

2.2. Results and Discussion

2.2.1. Optimization of CeO₂ Nanoparticle Synthesis

2.2.1.1. Effect of Synthesis Method

The XRD spectra and particle size distribution of synthesized CeO₂ nanoparticles are given in Figure 2.3. Although the crystals obtained were CeO₂ nanoparticles, the size distributions in monomer matrix were around 155 nm which corresponds to sub-micron level. Hence, this method was not selected as a synthesis method.

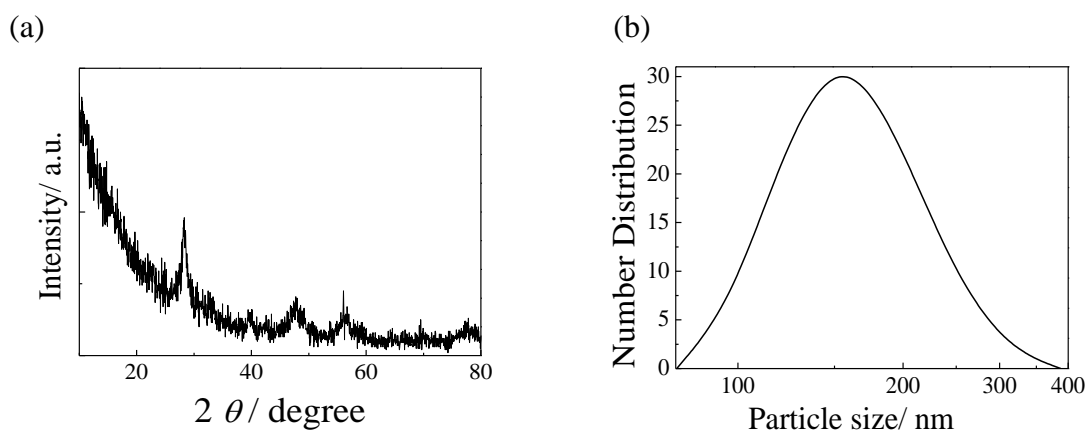


Figure 2.3. Characterization of CeO_2 particles obtained by hydrothermal synthesis (a) XRD diffractogram and (b) particle size distribution in monomer matrix.

The XRD diffraction pattern and particle size distribution of both unfunctionalized and surface functionalized CeO_2 particles are given in Figure 2.4. Since pure crystallites could not be obtained in MPS and TGA functionalized CeO_2 particles where cerium formate reflections were observed. The reason might be the chemical structures of surfactant molecules, and also the particle size distributions of all surface functionalized particles were greater than that of unfunctionalized ones, chemical precipitation method was not chosen as a synthesis method.

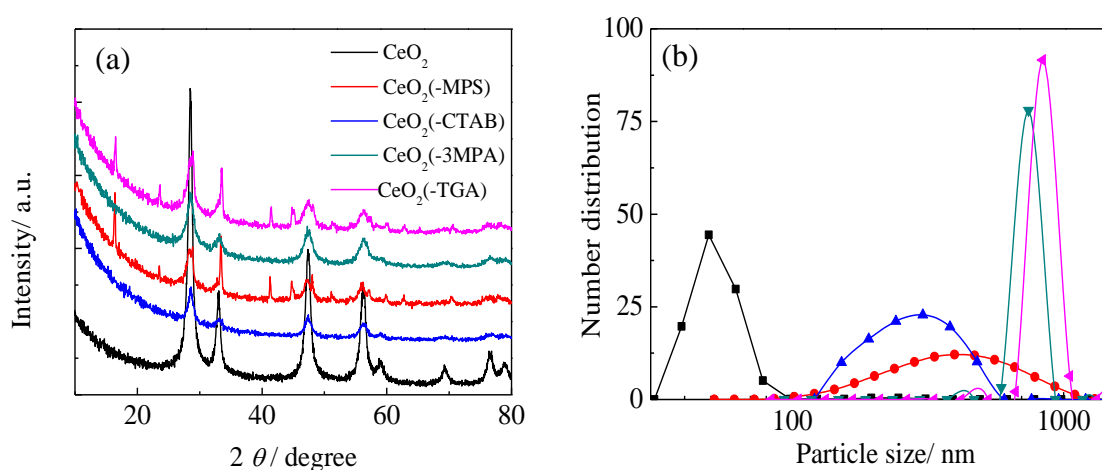


Figure 2.4. Characterization of CeO_2 particles obtained by chemical precipitation (a) XRD diffractogram and (b) particle size distribution in monomer matrix.

The formation of CeO_2 occurs in 3 subreactions (Eq 2.3). Hexamethylene tetraamine decomposes into ammonia and formaldehyde (Gorna et al., 2007) and

ammonia forms ammonium and hydroxide ions in water. CeO₂ particles are precipitated by the reaction of Ce(NO₃)₃ with excess hydroxide and oxygen gas which comes from air (Yang et al., 2007).



The growth of CeO₂ nanoparticles in absence and presence of surfactants is given in Figure 2.5. The addition of surfactant molecules cause shifts in UV-VIS spectra of nanoparticles. As the time passes, while addition of CTAB molecules cause a shift to higher wavelengths, a reverse effect is observed in TGA molecules.

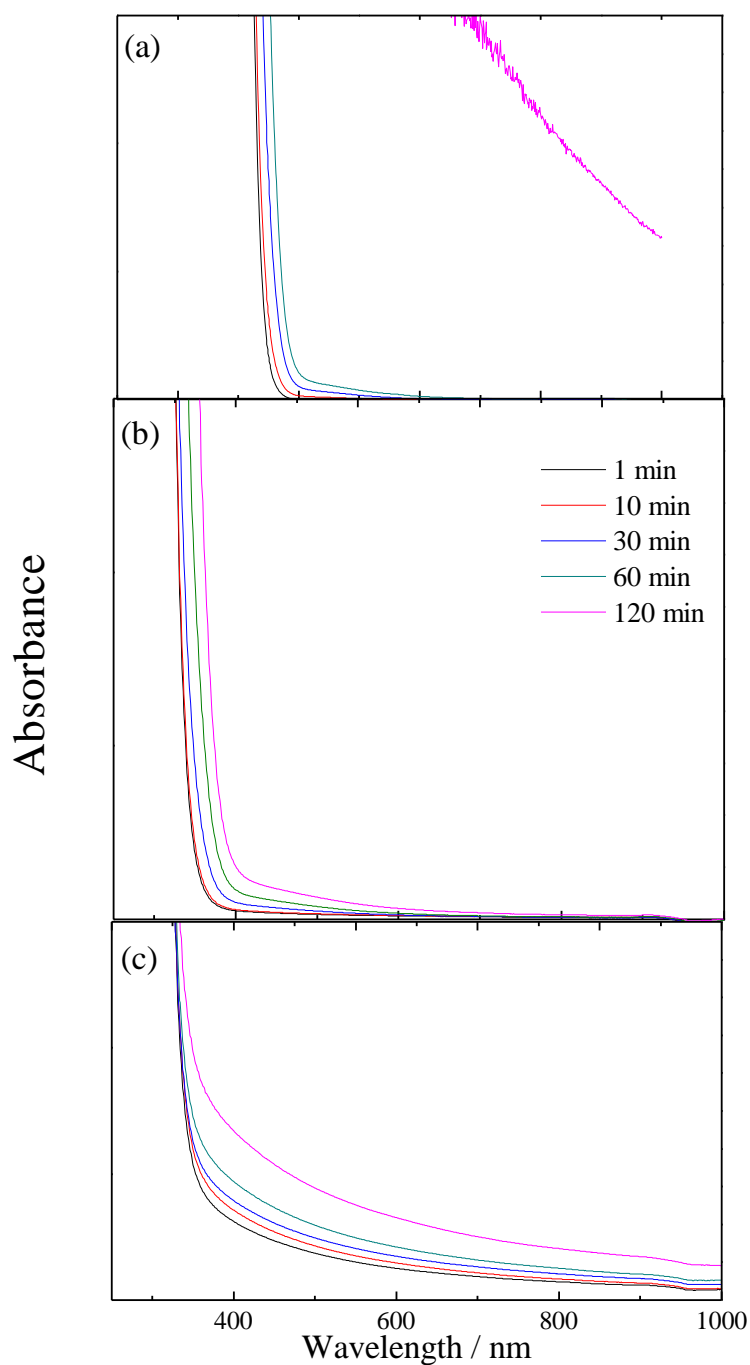


Figure 2.5. UV-VIS spectra of (a) CeO_2 synthesized by addition of CTAB, (b) CeO_2 and (c) CeO_2 synthesized by addition of TGA at room temperature and atmospheric pressure with HMTA as a precursor.

CeO_2 is a wide bandgap semiconductor. The particle size was estimated from blueshift of the absorption edge of UV-Vis light absorption edge (Zhang et al., 2004). The bandgap energy of nanoparticles, E^* , obtained from extrapolating linear portions of

the absorption edge and recording the intercepts with the energy axis. The bandgap energy of nanoparticles, E^* , is calculated by the formula:

$$E^* = E_g + \frac{\hbar^2 \Pi^2}{2R^2} \left[\frac{1}{m_e} + \frac{1}{m_h} \right] - \frac{1.8e^2}{\epsilon R} \quad (2.4)$$

In equation 2.4, E_g , R , m_e , and m_h are the bandgap energy, radius of nanoparticles, and effective masses of electron and hole, respectively. Bandgap energy of CeO_2 is 3.15 eV at room temperature, m_e and m_h are found as 0.4 m in literature where m is the mass of free electron (Zhang et al. 2002). In the equation, the value of ϵ is 24.5 which is the relative dielectric constant of CeO_2 . Zhang et al. calculated the optical band gap energy of ceria as $E_g=3.56$ eV that is blue-shifted when the value was compared with the bulk cerium oxide powders ($E_g= 3.19$ eV). As the typical size of the nanocrystals (3–5 nm) is far smaller than $2a_B$, in which the the value of exciton Bohr radius (a_B) value of the material was 7-8 nm, the optical bandgap shift categorized in strong confinement regime. In other words, the shift is mainly caused by quantum confinement that is inversely proportional to the square of the radius (Zhang et al. 2009). Effective mass model approach fails for the smallest ($r \leq 1$ nm) particles since the potential at the interface is infinitely high (Dieckmann et al. 2009). It was observed from experimental results that addition of surfactant is not so much effective on particle size growth within 10 minutes. As the time passes it was observed that, particle growth kinetics CeO_2 nanoparticles were favored by addition of the surfactants CTAB and 3-(mercaptopropyl) trimethoxy silane; however, it was slowed down by addition of 3MPA and TGA.

Growth kinetics of representative cerium oxide nanoparticles produced in absence and presence of MPS, CTAB, 3MPA or TGA is given in Figure 2.6. When the data obtained at 60 min were compared with each other, it was determined that MPS and CTAB enhanced the growth kinetics of cerium oxide nanoparticles; however, TGA and 3MPA slowed down the growth kinetics in the quantum regime of particles. Since the formula is applicable up to 10 nm particle size, it could not be possible to estimate the sizes of CeO_2 nanoparticles synthesized in presence of CTAB and MPS surfactants after 60 minutes.

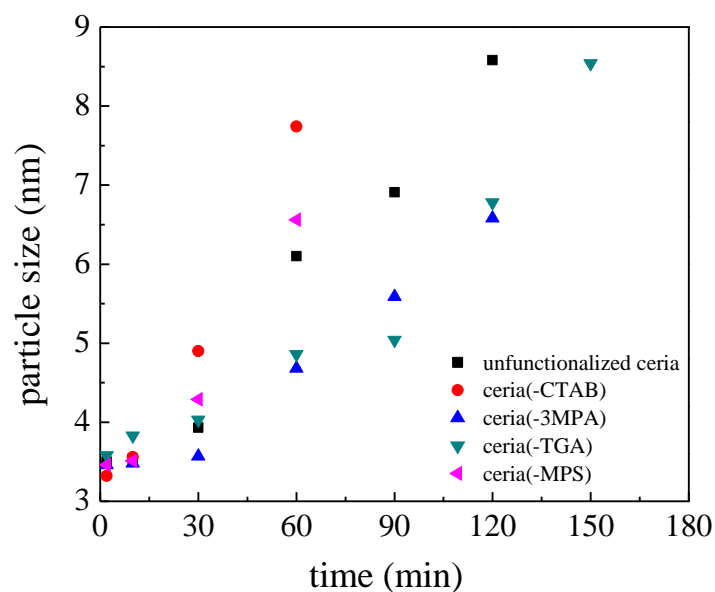


Figure 2.6. Particle size of CeO_2 nanoparticles synthesized by HMTA with respect to time (min) estimated from UV-VIS spectra. ■ unfunctionalized ceria, CeO_2 synthesized by addition of ● CTAB, ▲ 3MPA, ▼ TGA, and ◀ MPS.

Figure 2.7 shows X-ray diffraction (XRD) patterns of the CeO_2 nanoparticles precipitated in absence and presence of various surfactants. The reflecting planes (111), (200), (220) and (311) corresponding to the cubic fluorite structure are clearly observed.

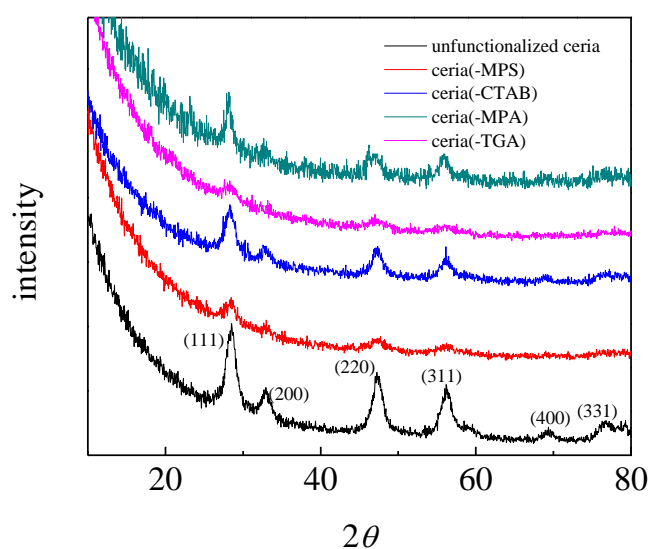


Figure 2.7. XRD pattern of CeO_2 particles synthesized by HMTA: unfunctionalized and functionalized particles in presence of MPS, CTAB, 3MPA, and TGA.

Cerium oxides can be either in the form of CeO_2 and Ce_2O_3 crystal form; hence, Z Wu et al. shows the differences of their characteristic XRD patterns (Z Wu et al., 2001).

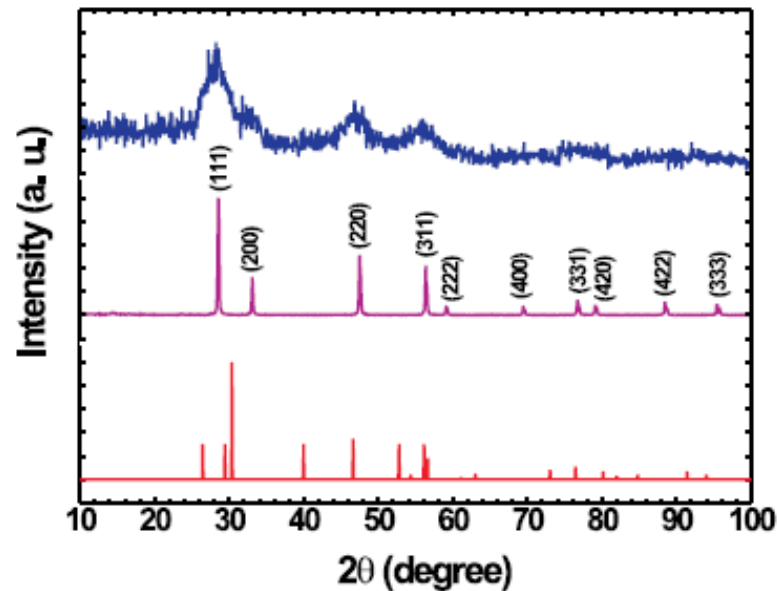


Figure 2.8. X-ray diffraction patterns of AOT-coated cerium oxide nanoparticles (top), bulk CeO_2 (middle) and bulk Ce_2O_3 (bottom) (Z Wu et al., 2001).

The reflections of CeO_2 and Ce_2O_3 are given in Figure 2.8. They involve no evidence of any diffraction reflections of Ce_2O_3 structure. The peak broadening with addition of surfactant in the diffraction pattern proves that obtained CeO_2 particles are smaller. It is stated that crystal size is estimated by utilizing Debye Scherer equation and the particle size estimated from band gap energy formula. The results are given in Table 2.1. It is observed that the particle size and the crystal size of synthesized nanoparticles are close to each other.

Table 2.1. Particle size and crystallite size values of each synthesized ceria nanoparticles by HMTA under ambient pressure and at room temperature. The particle size was estimated using Eq (2.1) at 1 hour and the size of crystals was obtained at 3 hours from XRD pattern by Debye-Scherrer.

SAMPLE	PARTICLE SIZE (nm)	CRYSTALLITE (nm)
CeO ₂	6.1	6.6
CeO ₂ -MPS	6.7	7.9
CeO ₂ -CTAB	7.7	6.2
CeO ₂ -3MPA	4.7	6.9
CeO ₂ -TGA	4.9	7.2

TEM images of unmodified CeO₂ particles and CeO₂ particles synthesized in the presence of CTAB are given in 2.9. It is clearly seen that the particle size of unmodified CeO₂ nanoparticles are less than that of CeO₂ particles synthesized in the presence of CTAB.

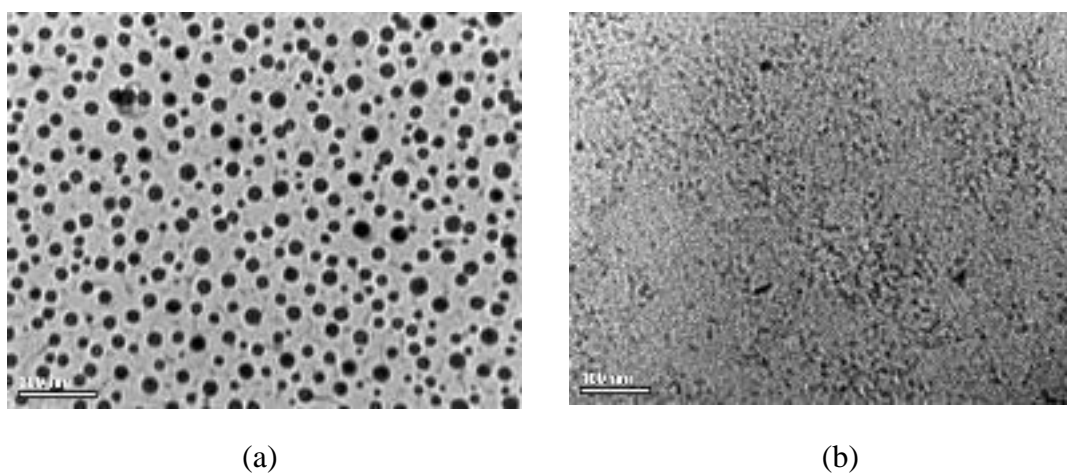


Figure 2.9. TEM images of CeO₂ particles synthesized by HMTA (a) unfunctionalized, and (b) functionalized by CTAB.

In order to determine the groups on the surface of CeO₂ nanoparticles, Diffuse Reflectance Infrared Fourier Transform (DRIFT) spectroscopy was utilized and

vibrational modes of organic groups around CeO₂ nanoparticles were recorded (Figure 2.10).

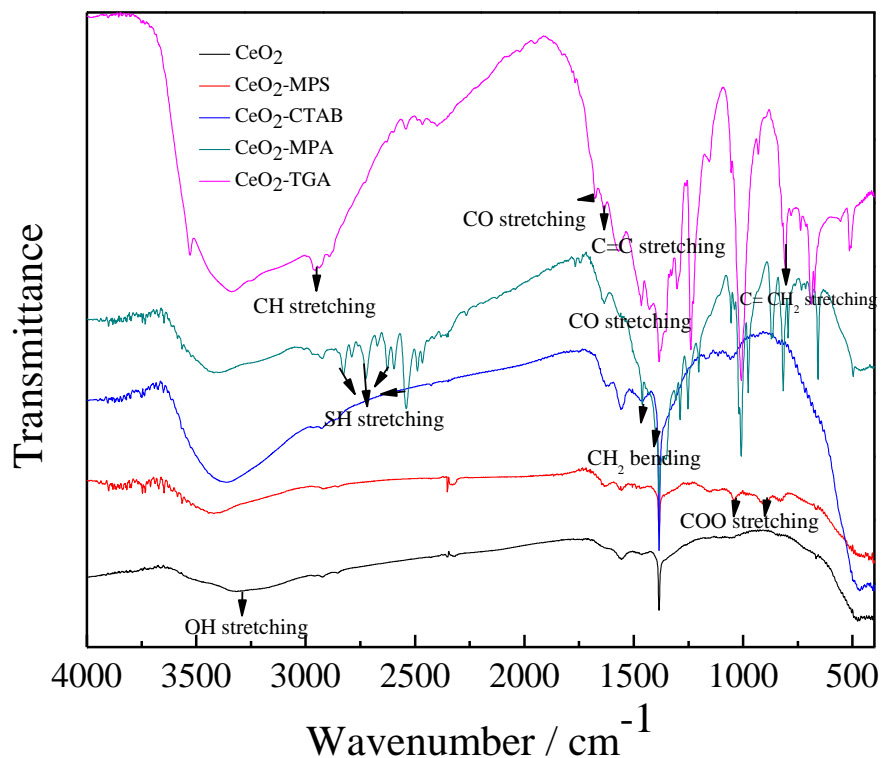


Figure 2.10. FTIR spectra of CeO₂ particles synthesized by HMTA: unfunctionalized and functionalized in presence of MPS, CTAB, 3MPA, and TGA.

Broad band centered around 3400-3300 cm⁻¹ is OH stretching. The band around 500 cm⁻¹ corresponds to the stretching vibration of Ce-O in CeO₂ structure (Taniguchi et al. 2008). Depending on chemistry of surfactants and chemical interaction between particle surface and surfactant, vibrational modes showed dissimilarities in the spectrum. Vibrations at the center of 1032 and 893 cm⁻¹ are COO stretching coming from the surfactant 3-(mercaptopropyl) trimethoxy silane. It was observed from the results that there was no difference between vibrational spectra of CeO₂ treated with and without hexadecyltrimethyl ammonium bromide (CTAB). Since there was no any symmetry change on CeO₂ vibrational modes after treated by CTAB, it was thought that the interaction between CeO₂ particles and CTAB might be electrostatic attraction between negatively charged oxygen of nanoparticle and positively charged nitrogen of CTAB. Vibrations around 2800-2500 cm⁻¹ and at the center of 1676, 1403, and 809 cm⁻¹ are SH stretching, CO stretching, CH₂ bending, and C=CH₂ stretching modes,

respectively coming from the structures of 3-mercapto propionic acid (3MPA) and thioglycolic acid (TGA).

Fluorescence spectrum of each nanoparticle was recorded in order to see the oxidation state of cerium in the synthesized nanoparticle which is demonstrated in Figure 2.11.

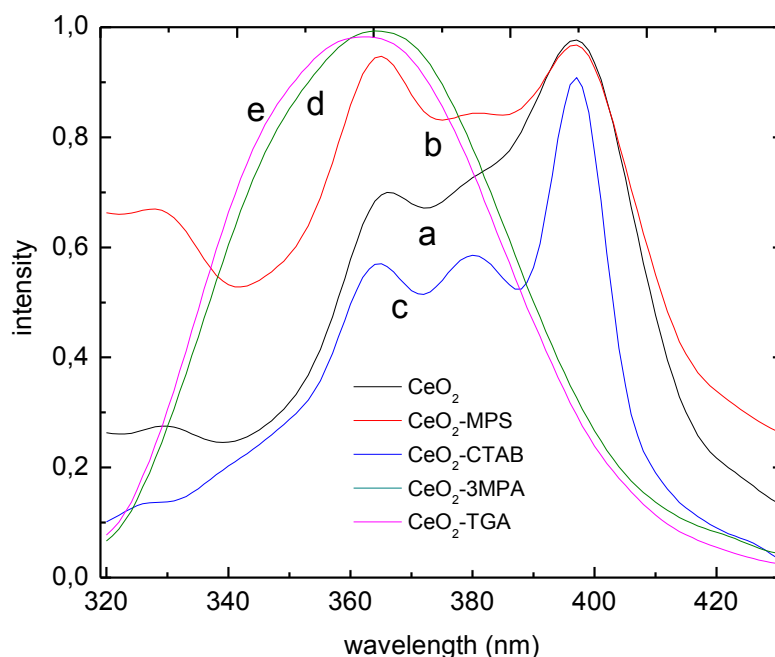


Figure 2.11. Fluorescence spectra of CeO_2 particles synthesized by HMTA (a) unfuntionalized, and functionalized in the presence of (b) MPS, (c) CTAB, (d) 3MPA, and (e) TGA.

It is known from literature that fluorescence of cerium obtained at 360 nm and 400 nm is coming from Ce^{3+} and Ce^{4+} species, respectively. In addition, the fluorescence coming from Ce^{3+} is called as a “defect”. It is obviously seen from the spectra that addition of 3-(mercaptopropyl) trimethoxy silane enhances the defect coming from Ce^{3+} ; nevertheless, this defect is reduced by addition of CTAB. On the other hand, the only species obtained by addition of 3MPA and TGA is Ce^{3+} . It is stated that Ce^{3+} sites are so active that they tend to adsorb and oxidize CO group (Matolín et al., 2009). According to fluorescence emission, it can be said that both unfuntionalized and functionalized CeO_2 nanoparticles involve is Ce^{3+} species. As the surfactants TGA

and 3MPA have both SH and OH ending groups, these surfactants are possibly bonded to CeO₂ surface from OH ending group with dissolution of OH and positively charged Ce³⁺ adsorbs negatively charged CO⁻ functional group.

Thermal degradation of synthesized cerium oxide nanoparticles was studied by thermogravimetric analysis (TGA) under nitrogen flow at a heating rate of 10° C min⁻¹. The TGA curve of each cerium oxide nanoparticles is given in Figure 2.12.

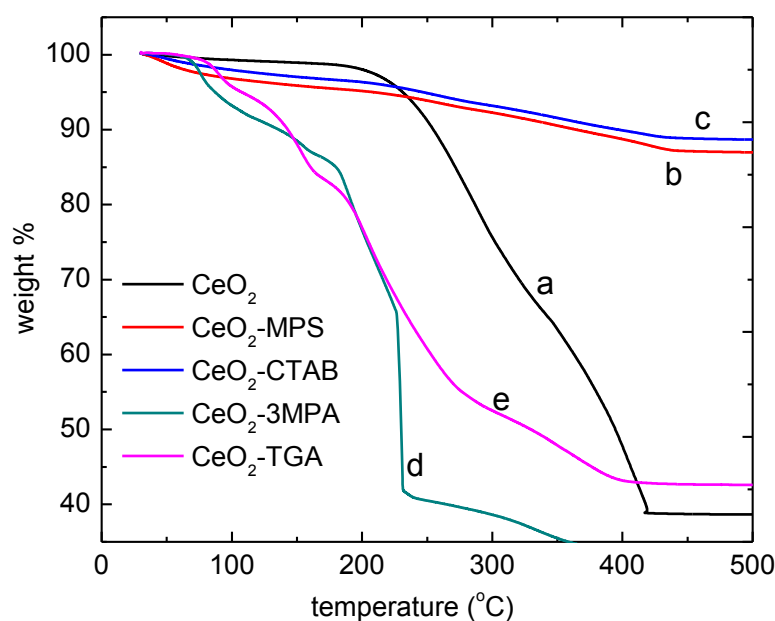


Figure 2.12. TGA curves of CeO₂ particles synthesized by HMTA (a) unfunctionalized and functionalized in the presence of (b) MPS, (c) CTAB, (d) 3MPA, and (e) TGA.

The weight loss of ceria nanoparticles synthesized by the addition of MPS and CTAB as a surfactant are 13 % and 11 %, respectively. The total weight loss of ceria nanoparticle is 61 %, whereas the ones synthesized by the addition of 3MPA and TGA as a surfactant are 59 % and 57 %, respectively. The reason of weight loss of neat CeO₂ nanoparticles might be excess HMTA molecules coming from precursor. In addition, the amount of organic species on CeO₂ nanoparticles synthesized by 3MPA and TGA are more than those of synthesized by MPS and CTAB molecules.

Size distribution of ceria nanoparticles in methyl methacrylate (MMA) were investigated by dynamic light scattering and the distributions are given in Figure 2.13.

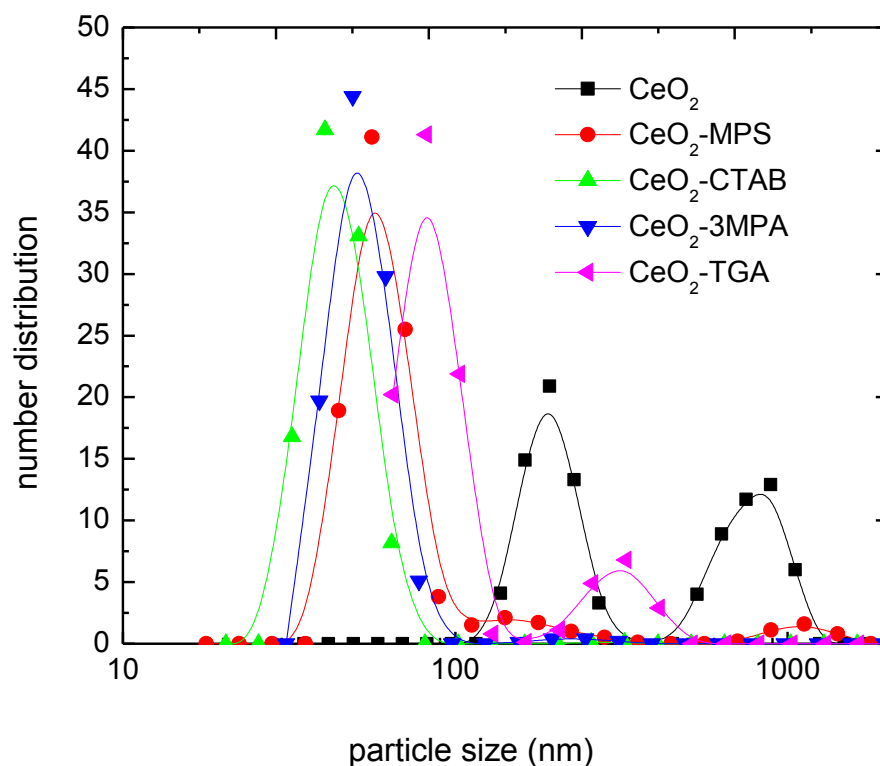


Figure 2.13. Particle size distribution of CeO_2 nanoparticle synthesized by HMTA (dispersed in methyl methacrylate) ■ unfunctionalized , functionalized by ● MPS, ▲ CTAB, ▼ TGA

According to the results obtained, the ceria nanoparticles had bimodal distribution except the ones synthesized by addition of CTAB and 3MPA as a surfactant. The ceria nanoparticles synthesized without any surfactant had a bimodal size distribution in 188 nm and 833 nm, respectively. The ceria nanoparticles synthesized by using MPS and TGA as surfactants had bimodal distributions in 56 nm, 1122 nm and 82 nm, 322 nm, respectively. The ceria nanoparticles synthesized by using CTAB and 3MPA as surfactants had particle size distributions with 40 nm and 49 nm sizes, respectively. These results indicated that, each surfactant provides a smaller particle size than that of the cerium oxide itself. The minimum size distribution was obtained by the cerium oxide nanoparticle which synthesized by using CTAB as a surfactant.

2.2.1.2. Effect of Reactant

Two kinds of cerium source, cerium nitrate hexahydrate ($\text{Ce}(\text{NO}_3)_3 \cdot 6\text{H}_2\text{O}$) and cerium acetate ($\text{C}_6\text{H}_9\text{CeO}_6 \cdot \text{H}_2\text{O}$) were treated with the base sources hexamethylene tetraamine (HMTA) and ammonium hydroxide (NH_4OH) solutions. XRD diffractogram of each synthesis method is given in Figure 2.14. Characteristic (111), (200), (220), (311), (400), and (331) reflections corresponding to the cubic fluorite structure of CeO_2 are clearly observed.

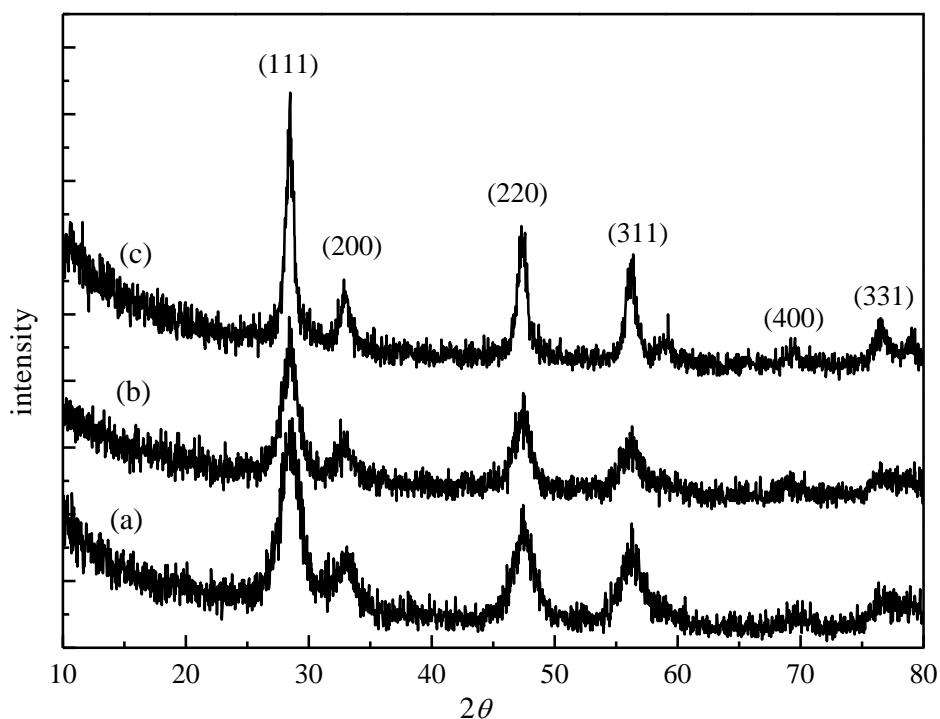


Figure 2.14. XRD pattern of CeO_2 particles synthesized by reacting reagent couples (a) cerium acetate-ammonium hydroxide, (b) cerium nitrate hexahydrate-hexamethylene tetraamine, and (c) cerium nitrate hexahydrate-ammonium hydroxide.

Percent yield of each synthesis method is given in Table 2.2. It is obvious that, ammonia solution enhances the formation of CeO_2 synthesis and the best yield obtained by reacting the reagents $\text{Ce}(\text{NO}_3)_3 \cdot 6\text{H}_2\text{O}$ and NH_4OH solutions.

Table 2.2. Percent yield values of CeO₂ obtained by reacting various reagents.

Reagents Used	Yield %
Ce(NO ₃).6H ₂ O-HMTA	5.0
CeAc-NH ₄ OH	16.0
Ce(NO ₃).6H ₂ O-NH ₄ OH	84.5

2.2.1.3 Effect of Reactant Ratio

In order to obtain high-yield pure CeO₂ particles, Ce(NO₃).6H₂O and NH₄OH are preferred as reacting reagents. As it is known from literature, the concentrations of reacting species directly affect the particle size; thus, the reacting ratio of Ce(NO₃).6H₂O and NH₄OH were chosen as 1:1, 1:5, and 1:10, separately. Results show that, nanometer sized CeO₂ particles can be obtained only when the mixing ratio is selected as 1:10. Former two give micron sized ceria nanoparticles.

The pH change for both unmodified- and modified-CeO₂ nanoparticles during synthesis is given in Figure 2.15. As soon as NH₄OH solution is added to Ce(NO₃).6H₂O solution, an abrupt pH drop is observed in the reaction system. Zhou et al. and Chen and Chen (Zhou et al. 2002, Chen and Chen 1993) reported that this sharp decrease is caused by the release of hydronium ions (H₃O⁺) during Ce(III)/Ce(IV) oxidation process by addition of higher concentration of hydroxyl ions. Hydroxyl ions are substantially consumed at a slower rate in the following hydrolysis and deprotonation steps. At the end of the reaction, pH values of both unmodified- and modified-CeO₂ nanoparticles are between 10.0 and 11.0 which demonstrates that dissolution and recrystallization process occur at basic conditions.

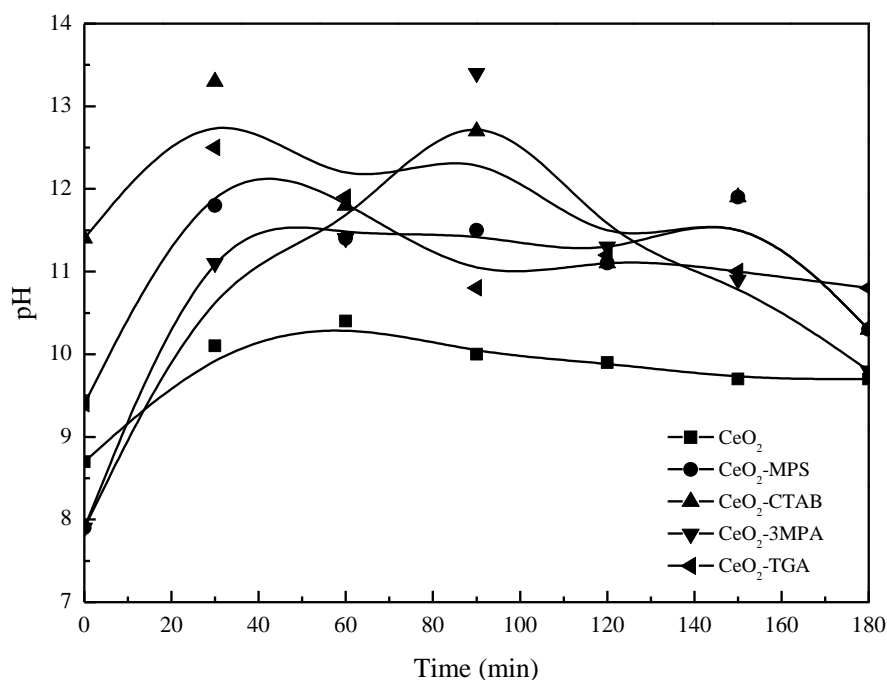


Figure 2.15. pH change of both unfunctionalized- and functionalized-CeO₂ nanoparticles during synthesis.

2.2.1.4. Effect of Reaction Temperature

In order to observe the effect of temperature change on the synthesis of nanosize ceria particles, two different temperatures, 22 °C and 30 °C, were applied without changing any other parameters. It is clearly observed that, when the temperature is selected as 30 °C, micron sized ceria particles were obtained instead of nanosized ceria particles. Hence, size of synthesized particles increase as the reaction temperature is increased.

2.2.1.5. Effect of Direct and Reverse Strike

In order to obtain high yield of nanosized CeO₂ particles, both direct and reverse strike methods were applied. In direct strike, NH₄OH was added into Ce(NO₃)₃·6H₂O precursor dropwise; whereas, in reverse strike vice versa. Although the yields of each method was close to each other, the particle size obtained from direct strike method was

less than that of reverse strike. Therefore, direct strike was selected as a synthesis method in this study.

2.2.2. Characterization of CeO₂ Nanoparticle

X-ray diffraction (XRD) patterns of both in situ and ex situ functionalized CeO₂ nanoparticles are given in Figure 2.16. The reflections are same with those of cubic ceria (JCPDS Card No. 81-0792) which are shown as vertical drop lines at the bottom of the pattern.

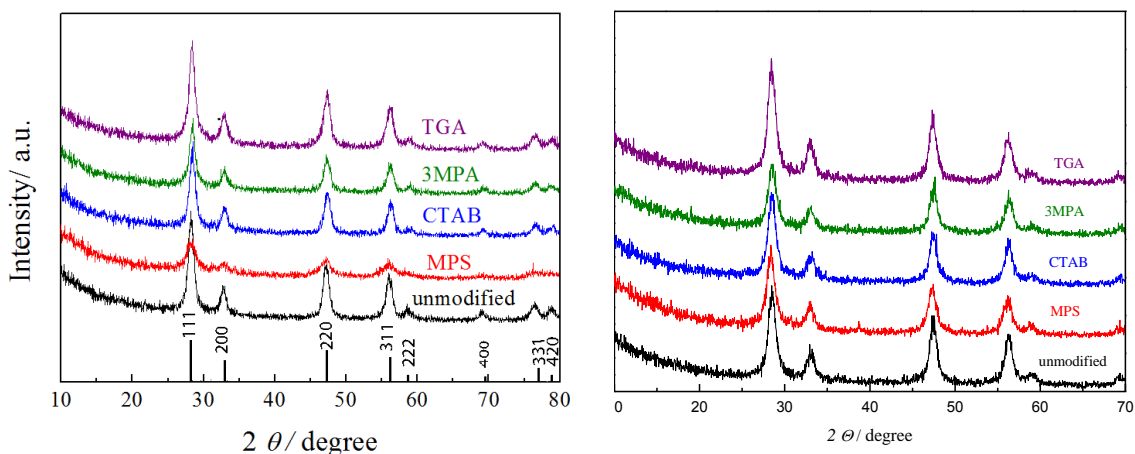


Figure 2.16. XRD pattern of CeO₂ particles synthesized by NH₄OH (a) in situ and (b) ex situ synthesized

The crystallite sizes of both in situ and ex situ functionalized CeO₂ particles estimated by using Debye-Scherrer's equation are given in Table 2.3. The crystallite of in situ functionalized particles is less than that of ex situ functionalized ones. In situ particle functionalization is more effective since the particle growth occurs in presence of modifiers; so, it decreases the crystal growth of particles. However, ex situ functionalization is performed after the growth of neat ceria particles; hence, it has no remarkable effect on crystal growth.

Table 2.3. Crystallite values of the ceria nanoparticles synthesized by NH_4OH under ambient pressure and at room temperature. The size of crystals was obtained from XRD pattern by using Scherrer's equation taking into account (111) reflection.

Sample Name	Crystallite (nm)	
	in situ functionalized	ex situ functionalized
ceria	8	11
ceria(-MPS)	4	11
ceria(-CTAB)	10	9
ceria(-3MPA)	6	11
ceria(-TGA)	6	10

The formation of cubic fluorite structure of ceria is developed from either spherical (Niesz et al. 2010) or rod-like (Wang and Feng 2003) morphology to truncated octahedral. Then, it is gradually converted to a cubic shape independent of initial morphology. Figure 2.17 contains overview of TEM micrographs of both in situ and ex situ synthesized CeO_2 nanoparticles, respectively. Average size of nanoparticles is estimated by measuring the size of more than 50 particles in the TEM micrographs and is given in Table 2.4. It is clear from results that an average size of in situ synthesized particles is about 5 nm whereas ex situ synthesized ones are varying from 4 nm to 9 nm.

Table 2.4. Crystallite values of synthesized ceria nanoparticles obtained by TEM micrographs.

Sample Name	Crystallite (nm)	
	in situ functionalized	ex situ functionalized
ceria	5 ± 2	4 ± 1
ceria(-MPS)	4 ± 2	5 ± 2
ceria(-CTAB)	6 ± 1	5 ± 1
ceria(-3MPA)	4 ± 1	5 ± 1
ceria(-TGA)	5 ± 3	8 ± 2

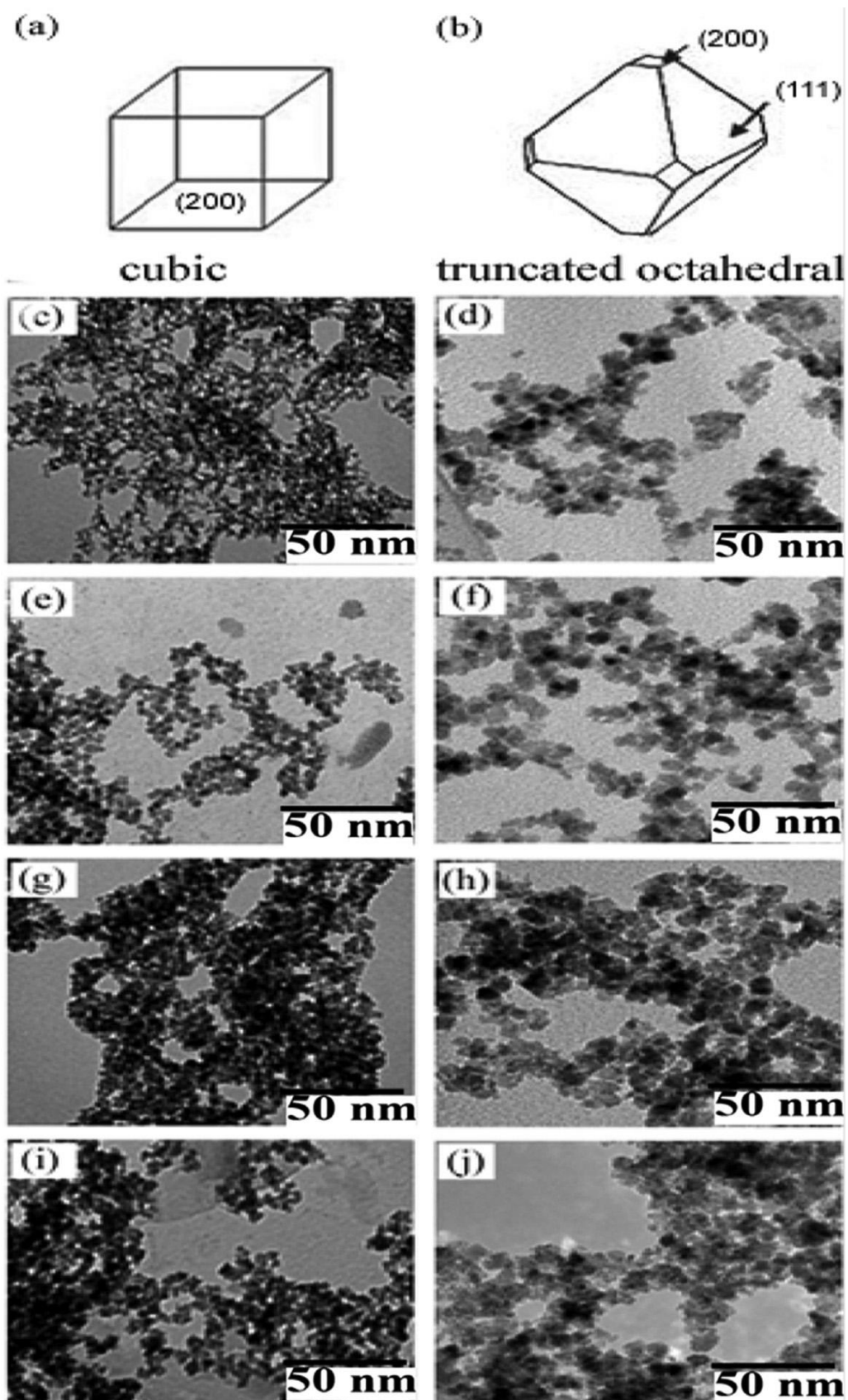


Figure 2.17. Structural models of (a, b) in situ and ex situ functionalized particles and TEM micrographs of in situ and ex situ (c, d) MPS, (e, f) CTAB, (g, h) MPA, and (i, j) TGA functionalized CeO₂ nanoparticles synthesized by NH₄OH.

The morphology of in situ synthesized nanoparticles is investigated in detail by taking high resolution TEM micrographs. In order to reduce the surface area / volume ratio, the unmodified particles show great tendency to aggregate. Hence, it is hard to take images of individual unmodified particles. High resolution TEM micrographs of unfunctionalized, CTAB- and MPS-functionalized aggregated particles demonstrated in Figure 2.18. As seen in the figure, unfunctionalized CeO₂ particles aggregate and possess cuboctahedral shape whereas, CTAB- and MPS-functionalized particles show cubic morphology. Each particle is a well ordered single crystal possessing 0.31 nm fringe distance corresponding to (111) lattice of ceria. The distances 0.26 nm, 0.13 nm and the ones ranging from 0.19 nm and 0.23 nm are corresponding to (200), (400), and (220) lattices of ceria. The crystal sizes of synthesized ceria nanoparticles are obtained by measuring 20 nanoparticles from micrographs of TEM are given in Table 2.4. It is obvious that there is no excessive difference between the crystallites of unfunctionalized, in situ and ex situ functionalized ceria nanoparticles.

The precipitation reaction yield of both synthesis methods is estimated gravimetrically. According to the calculations, the yield of in situ functionalized ceria nanoparticles lie between 50 and 70%, whereas, the ones synthesized by ex situ functionalization lie between 75 and 95%. The difference may be due to the effect of surfactant molecules in in situ functionalization which might slow down the growth kinetics of the particle formation.

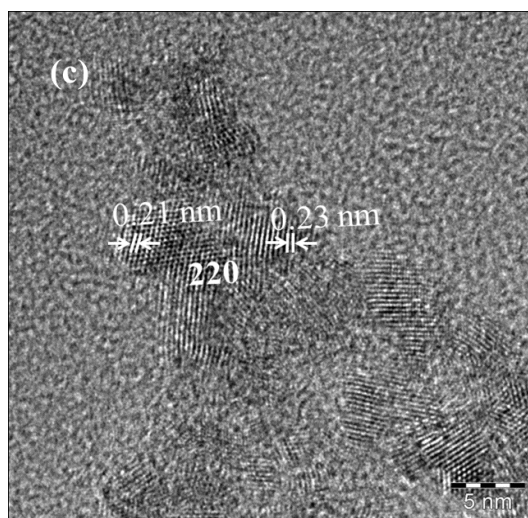
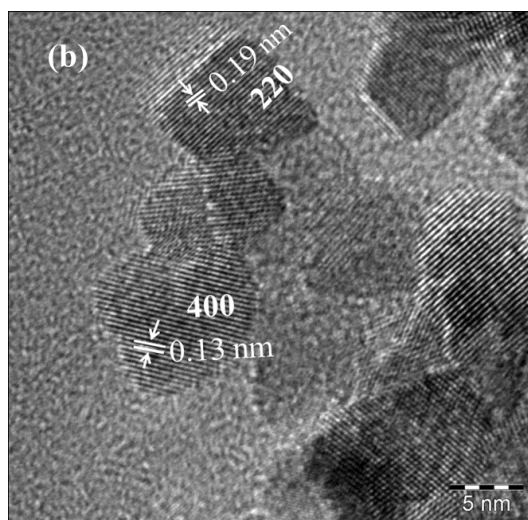
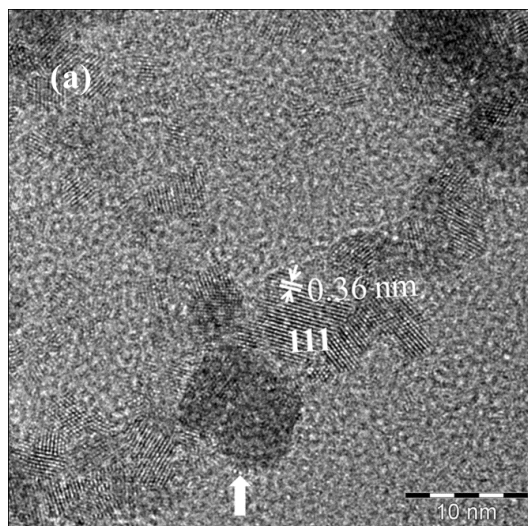


Figure 2.18. High resolution TEM micrographs of CeO_2 particles synthesized by NH_4OH : (a) unfunctionalized and in-situ functionalized by (b) CTAB, (c) MPS.

2.2.3. Surface Chemistry and Stability of Particle Dispersion

The control of the surface chemistry is important for both the compatibility of the particles with organic media and reaching certain properties such as hydrophobicity, surface charge, roughness, surface energy, and reactivity. In order to examine the functional groups present on the surface of CeO₂ nanoparticles, both Fourier transform infrared (FTIR) spectroscopy and nuclear magnetic resonance (NMR) are performed. FTIR spectra of unfunctionalized, in situ and ex situ functionalized CeO₂ nanoparticles are presented in Figure 2.19.

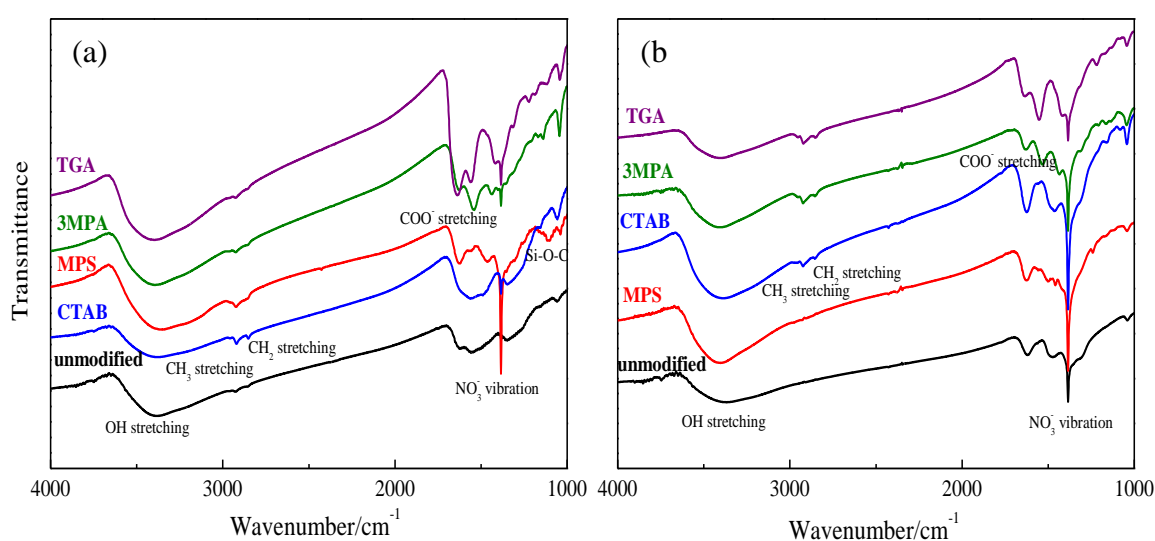


Figure 2.19. FTIR spectra of CeO₂ particles as-synthesized by NH₄OH (a) in situ functionalized and (b) ex situ functionalized.

Two signals, broad bands centered around 3300-3400 cm⁻¹ and a narrow peak at 1384 cm⁻¹, are commonly observed in all spectra. The former band is attributed to OH stretching but the latter peak is originating from nitrate groups. When the spectra of the surface-functionalized particles are compared with that of the corresponding pure surfactant, the appearance or disappearance of characteristic signals of surfactant molecules demonstrate the grafting of surfactant molecules on the particle surface. For TGA and MPA, the SH band at 2800-2500 cm⁻¹ disappears while the bands of COO⁻ group remains at 1676 cm⁻¹. The reason of disappearance of SH band could be a condensation reaction between SH and surface of OH groups, leading to a grafting of the molecules to the particle surface. Also, when MPS is used as a surfactant, a new band attributed to the Si-OC bond appears around 1153 cm⁻¹. For CTAB-capped

particles, a remarkable enhancements are observed in the vibrations of CH₂ bending at 1346 cm⁻¹ after modification. This might be caused by the Coulombic interaction between quaternary ammonium salt and ceria surface.

Chemical shifts and full width half maximum values of vibration bands are estimated and given in Table 2.5. The changes to lower wave numbers show that the energies of vibrations decrease because of the bond formation between CeO₂ surface and surfactant molecules. SH vibrations except the ones functionalized by 3MPA are observed in neither in situ nor ex situ functionalized CeO₂ nanoparticles. Absence of these vibrations is the evidence of the grafting of the surfactant molecules from SH-end. On the other hand, approximately 200 cm⁻¹ shift in the stretching vibration of COO⁻ functional group is observed for both 3MPA and TGA modified CeO₂ particles. Moreover, a band broadening is seen in FTIR spectrum of COO⁻ vibration in in situ functionalized particles whereas, this vibration is sharpened in ex situ functionalized ones. Furthermore, the vibration approximately 1100 cm⁻¹, coming from Si-O-C bond of MPS is both observed in neat surfactant and in situ functionalized particles. In contrast, this vibration is not observed in ex situ functionalization. This result proves that while in situ functionalization is successful, there is no any surface functionalization in ex situ functionalized particles. Additionally, the presence of nitrate groups around 1384 cm⁻¹ in all functionalized particles shows that a complete packaging on the surface particles cannot be achieved.

Table 2.5. Vibrational band shifts and full width half maximum (FWHM) values of FTIR bands

VIBRATION	PURE SURFACTANTS			IN SITU FUNCTIONALIZED CeO ₂			EX SITU FUNCTIONALIZED CeO ₂		
		SHIFT	FWHM		SHIFT	FWHM		SHIFT	FWHM
CH ₃ STRETCHING	CTAB	2919	17.9	CeO ₂ CTAB	2920	22.5	CeO ₂ CTAB	-	-
SH STRETCHING	MPS	2854	80.3	CeO ₂ MPS	-	-	CeO ₂ MPS	-	-
	3MPA	2850	14.4	CeO ₂ 3MPA	2855	8.3	CeO ₂ 3MPA	2855	8.2
	TGA	2850	7.1	CeO ₂ TGA	-	-	CeO ₂ TGA	-	-
COO ⁻ STRETCHING	3MPA	1699	42.0	CeO ₂ 3MPA	1541	53.7	CeO ₂ 3MPA	1554	34.8
	TGA	1702	88.5	CeO ₂ TGA	1589	136.5	CeO ₂ TGA	1553	47.7
Si-O-C STRETCHING	MPS	1153	27.7	CeO ₂ MPS	1111	29.5	CeO ₂ MPS	-	-
NO ₃ ⁻ STRETCHING		-	-	CeO ₂	1384	4.9	CeO ₂	1384	6.3
	MPS	-	-	CeO ₂ MPS	1385	8.4	CeO ₂ MPS	1384	7.6
	CTAB	-	-	CeO ₂ CTAB	1385	5.5	CeO ₂ CTAB	1384	14.0
	3MPA	-	-	CeO ₂ 3MPA	1384	6.1	CeO ₂ 3MPA	1383	10.7
	TGA			CeO ₂ TGA	1384	6.1	CeO ₂ TGA	1385	67.8

The utilization of ¹³C CP-MAS NMR spectroscopy performed at low temperatures (~100K) is demonstrated for two selected synthesized nanomaterials, in situ MPS and 3MPA functionalized CeO₂ particles in Figure 2.20. The spectra are recorded at ~100 K, ~9 kHz MAS and in ~12 h each.

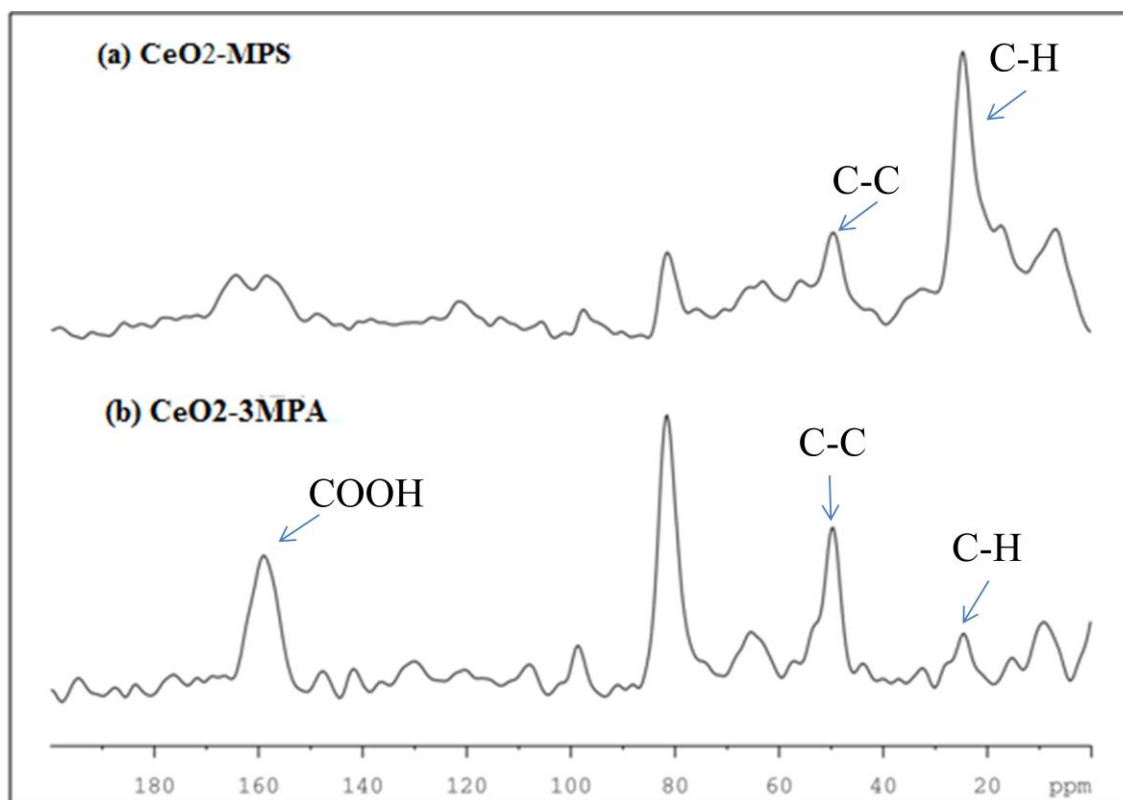


Figure 2.20. ^{13}C CP-MAS spectrum of CeO_2 particles synthesized by NH_4OH : in situ surface functionalized in the presence of (a) MPS, and (b) 3MPA.

The successful functionalization of the surface of nanomaterial with MPS and 3MPA is proved by clear signals from surface surfactant species those are from CH_2 and carboxylic carbon sites. The signals at 30 and 50 ppm correspond to C-H and C-C, respectively. A sharp signal around 160 ppm shows the presence of COOH site.

The preparation method and starting materials give different nucleation and growth behaviors to the synthesized CeO_2 nanoparticles even though the product possesses identical features in the bulk. This difference in the crystal growth causes defects in the structure. Electronic transitions and optical properties are strongly affected from crystal defects. Room-temperature photoluminescence (PL) spectra of in situ synthesized samples are demonstrated in Figure 2.21.

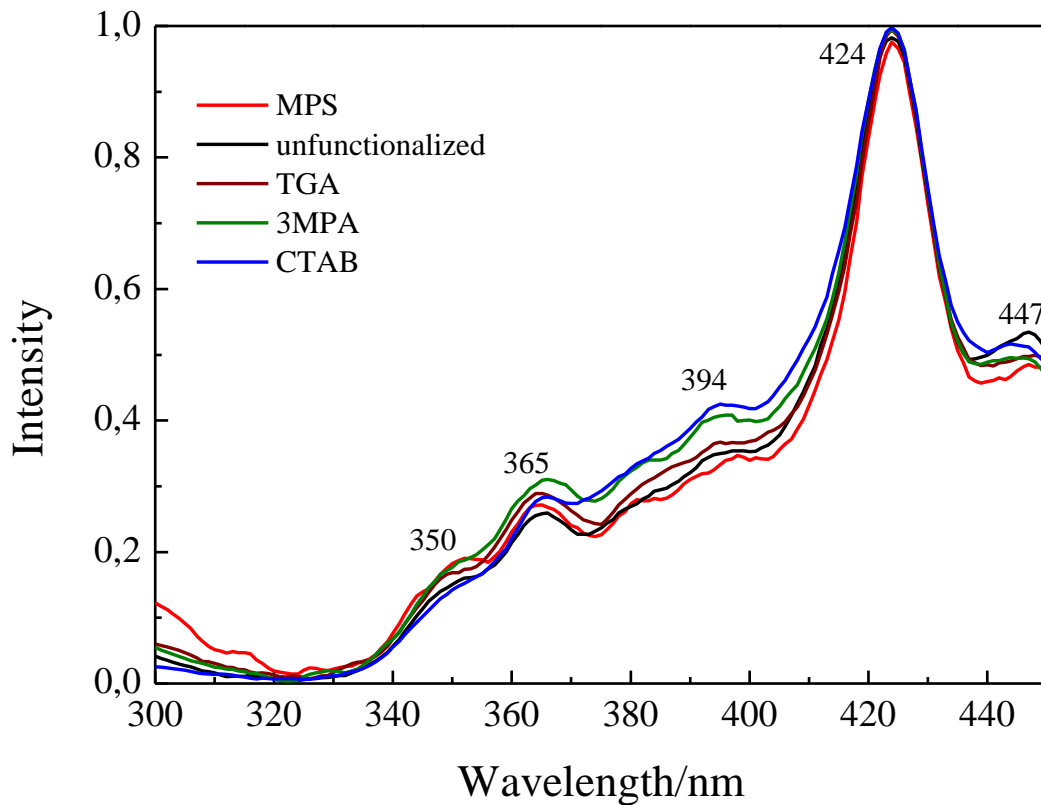


Figure 2.21. Fluorescence spectra of CeO₂ nanoparticles in situ synthesized by NH₄OH.

Photoluminescence spectra exhibit that there isn't significant difference between unfunctionalized and surface-functionalized particles, meaning that optical properties are not affected by the presence of surfactant molecules. Photoluminescence emissions at around 424 nm, 395 nm, and two broad emissions around 365 nm and 350 nm are observed in both unfunctionalized and functionalized CeO₂ nanoparticles. In order to investigate the effects of surfactants on the emission, the spectra are normalized concerning the most intense signal at 424 nm. The emission bands at 424 nm and 394 nm correspond to the charge transfer from O₂ to Ce⁴⁺, that is, charge transfer or electron transition from oxygen vacancies (Lu et al. 2009, Maensiri et al. 2007, Sun et al. 2005). Charge transfer transition from O²⁻ to Ce⁴⁺ is demonstrated by the two weak and broad signals at 365 nm and 350 nm (Palard et al. 2010, Sujana et al. 2008).

Thermal degradation of both in situ and ex situ synthesized cerium oxide nanoparticles under nitrogen flow is studied by thermogravimetric analysis and given in Figure 2.22.

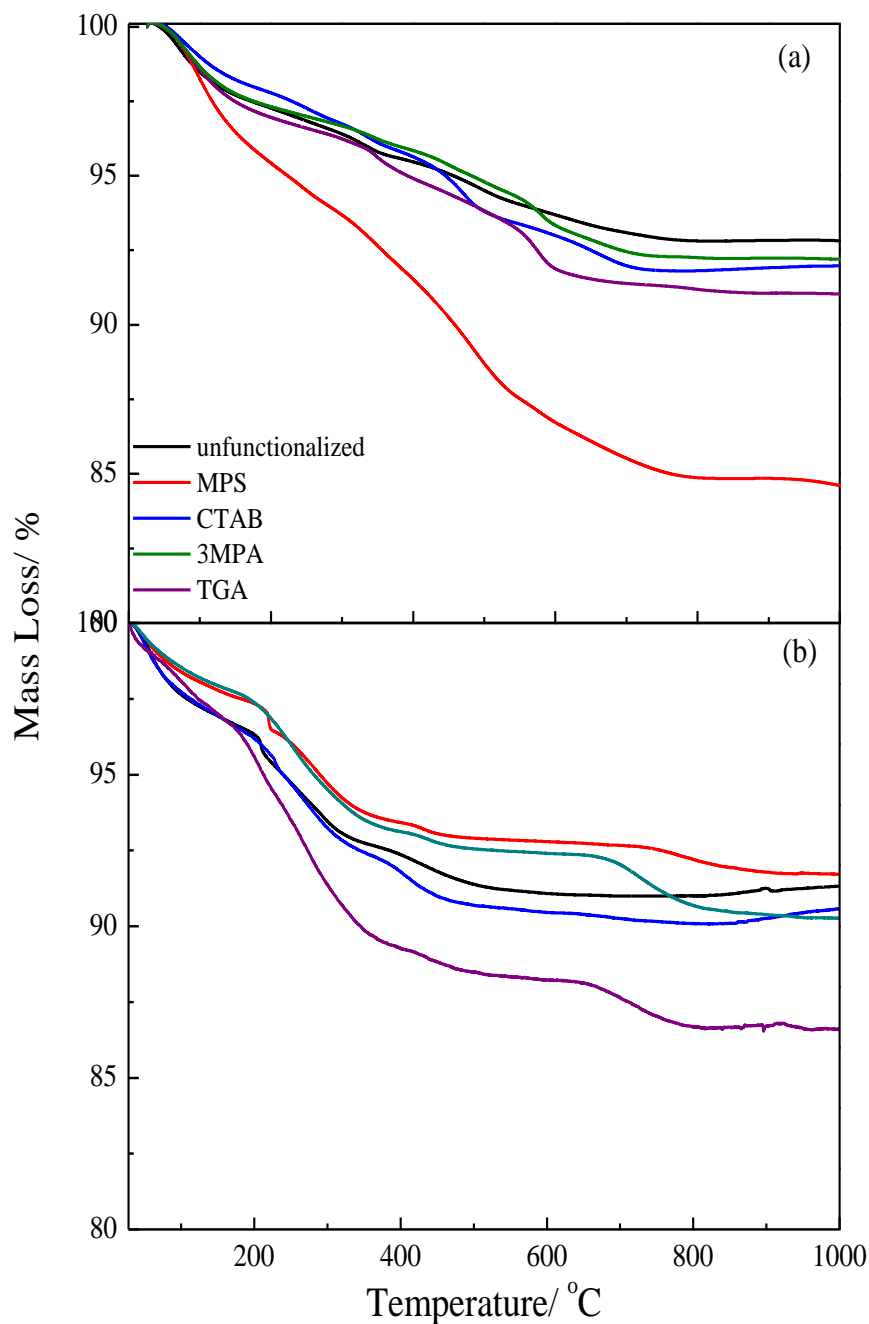


Figure 2.22. Mass loss curves of the CeO_2 particles as-synthesized by NH_4OH (a) in situ functionalized and (b) ex situ functionalized.

A continuous mass loss is investigated until ca. 800°C for both in situ and ex situ synthesized CeO_2 nanoparticles. After that temperature, the curves reach a plateau for in situ functionalized particles which corresponds to ca. 93% and 85-92% loss for unfunctionalized and surface-functionalized particles, respectively. The content of organic component in the sample is estimated from mass loss difference between unfunctionalized and functionalized samples that ranges from 0.6 wt% to 7.8 wt% for

3MPA and MPS, respectively. The mass loss of both in situ and ex situ CTAB-functionalized CeO₂ nanoparticles are demonstrated at Figure 2.23.

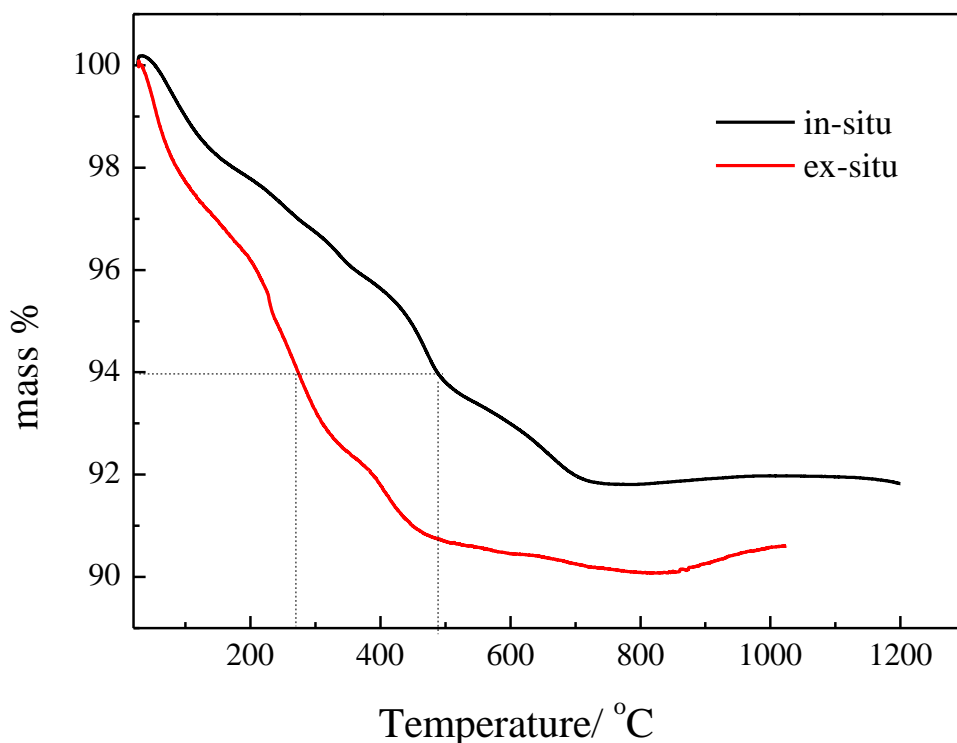


Figure 2.23. Thermogram of in situ and ex situ CTAB-capped ceria particles.

The mass loss of synthesized nanoparticles demonstrate discrepancies depending on the synthesis method. For instance, 6 % mass loss both in situ and ex situ ceria (-CTAB) functionalized particles is observed at 500 °C and 300 °C, respectively. This result shows that in situ functionalized particles are thermally more stable than that of ex situ functionalized ones which proves that the capping agents are more tightly adsorbed to the particle surface in the process of in situ functionalization (Tunusoğlu et al. 2012).

Surface charge is one of the most important properties of nanoparticles for the stability of dispersions. The ionization of surface groups or the adsorption of cations or anions change the surface charge of nanoparticle when it is dispersed in an aqueous solution. Hence, an electrical potential between the particle surface and the dispersion medium is established. The electrostatic repulsion force between colloidal particles and the medium is determined by zeta potential measurements. The isoelectric point (IEP) is defined as the point at which the surface charge is zero, is also provided by these measurements. The chemistry of surfactant changes the surface charge. The effect of pH

values on zeta potentials of in situ synthesized both unfunctionalized and functionalized CeO₂ nanoparticles is demonstrated at Figure 2.24.

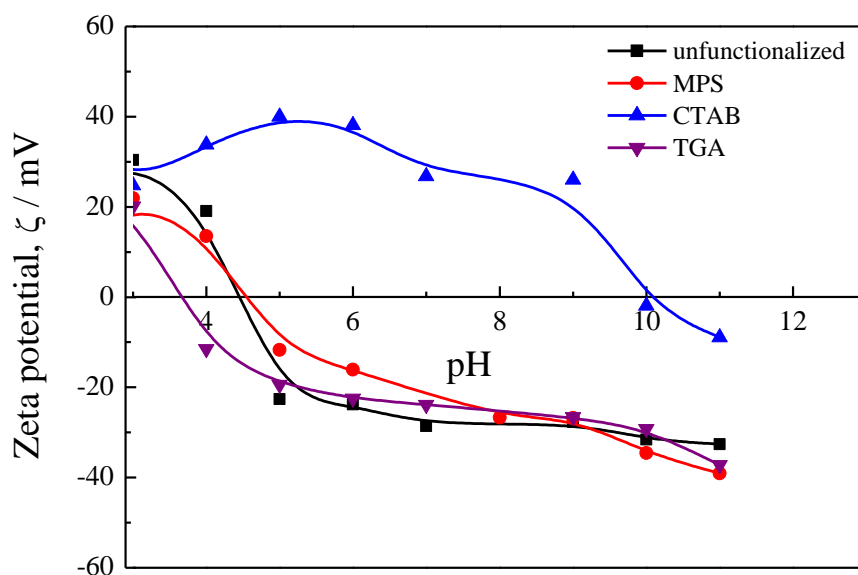


Figure 2.24. Zeta potentials of CeO₂ particles synthesized by NH₄OH: in situ unfunctionalized and functionalized particles in presence of MPS, CTAB, and TGA dependent on pH values.

The surface charge ranges from positive to negative with the increase of pH in consequence of the deprotonation of the surface groups. The isoelectric point for unfunctionalized particles is 4.4, which shows that the surface of unfunctionalized CeO₂ particles is negative. Israelachvili states that hydroxyl groups generally cover the surface of metal oxide nanoparticles dispersed in water (Israelachvili J.N. 2011). The origin of negative surface charge might be the partial dissociation of hydroxyl groups. Hence, the usage of positively charged surfactant, such as CTAB, causes a shift to higher pH value (pH=9.9) of isoelectric point on account of Coulombic interaction between the negative sites on the particles. The utilization of MPS possessing silane groups, cannot affect the surface charge. Since the grafting occurs through surface hydroxyl groups, the charge balance on the particle surface is not affected. When TGA is used as a surfactant, the isoelectric point decreases to lower pH values. According to the FTIR spectra, grafting of TGA molecules onto the particle surface mainly occurs by condensation of -SH and surface of -OH groups. Thus, carboxylic acid group of the surfactant molecule is observed on the particle surface. Since this group dissociates and forms carboxyl species in aqueous medium, the surface becomes more negative and the

isoelectric point decreases to lower pH value (pH=3.8). The selection of surfactant designates the control of surface charge.

Particle size distributions of unfunctionalized, in situ, and ex situ functionalized CeO₂ nanoparticles in monomer methyl methacrylate (MMA) are investigated by dynamic light scattering (DLS) and the results are given in Figure 2.25.

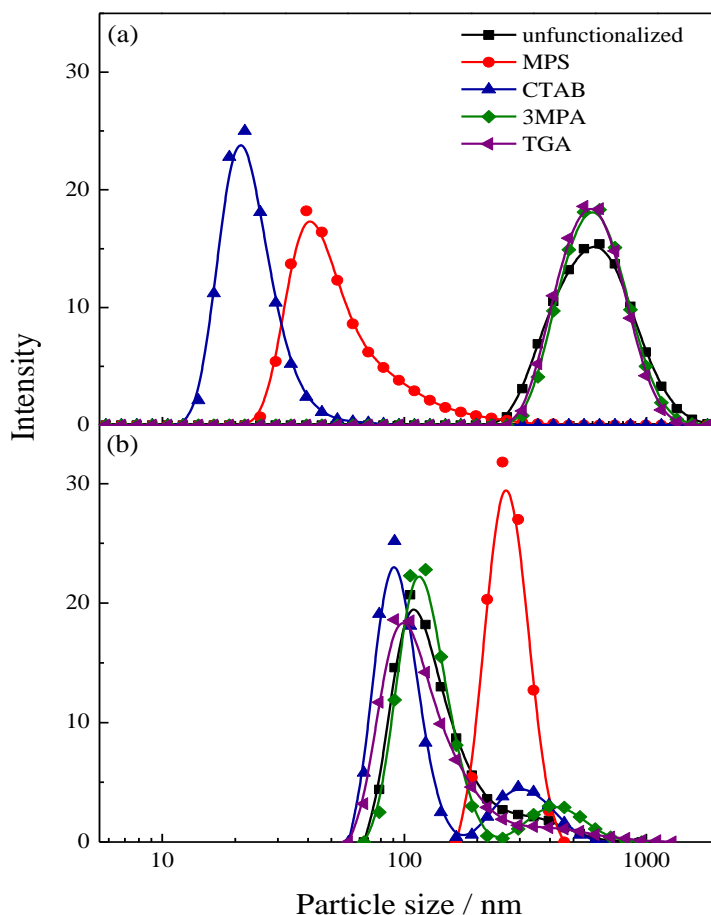


Figure 2.25. Particle size distributions of unfunctionalized and functionalized CeO₂ nanoparticles synthesized by (a) in situ and (b) ex situ method.

The unfunctionalized CeO₂ particles demonstrates large particle domains because of the surface hydroxyl groups. Since strong hydrogen bonding interactions occur between particles and the surrounding monomer, these groups cause particle aggregation. Hence, surface-capped molecules are used to prevent this aggregation and allow CeO₂ nanocrystals redisperse in organic media. The surface chemistry of particles is important for interactions between nanocrystals and organic media and dispersion stability. The unfunctionalized ceria particles demonstrate mean diameter of 600 nm

and 110 nm for in situ and ex situ synthesis methods, respectively. The reason of this difference might be the synthesis methods. The mean diameter values of both in situ and ex situ synthesized particles are given in Table 2.6.

Table 2.6. Mean diameter values of both in situ and ex situ synthesized particles obtained from DLS in MMA.

	mean diameter (nm)	
	in situ	ex situ
unfunctionalized ceria	600	110
ceria(-MPS)	40	260
ceria(-CTAB)	20	90
ceria(-MPA)	600	120
ceria(-TGA)	600	100

For in situ synthesis method, the particles functionalized by MPA and TGA show comparable particle size distributions with the unfunctionalized ones. Both surfactant molecules possess mercapto and carboxyl groups. Both functional groups may coexist on the surface even though the molecules are attached from mercapto groups. Since the surface possess hydrophilic nature because of the presence of carboxylic acid groups, the compatibility with the hydrophobic MMA medium is reduced. Thus, these two surfactants are not good choices for homogeneous dispersion in organic media. On the other hand, the particles functionalized with MPS and CTAB have average particle sizes of 40 nm and 20 nm, respectively. In MPS, the self-condensation of silane groups causes the formation of high amount of SiO₂ network (Chang et al. 2008). According to the average particle size values, the surfactant CTAB

is the best choice within the other applied surfactant molecules. CTAB is attached to CeO₂ surface from its cationic part via electrostatic attraction as the surface of nanoparticle has a negative potential. Therefore, surface hydrophobicity is provided by the long hydrophobic alkane group and the smallest particle size is obtained. On the other hand, the domain size of ex situ functionalized particles is varying from 100 nm to 250 nm. This result shows that, ex situ functionalization is not as sufficient as in situ method.

The graft density of capping agents on the particle surface is estimated from mass loss of capping agents and XRD crystallite sizes from Debye Scherrer equation assuming monolayer coverage on the spherical ceria particles. The graft densities of capping agents for both in situ and ex situ synthesized particles are listed in Table 2.7.

Table 2.7. Graft density estimated by thermogravimetric analysis and particle size

	graft density (molecules/nm ²)	
	in situ	ex situ
unfunctionalized ceria	no grafting	no grafting
ceria(-MPS)	2.5	negligible grafting
ceria(-CTAB)	0.9	0.13
ceria(-MPA)	2.4	0.8
ceria(-TGA)	4.1	3.9

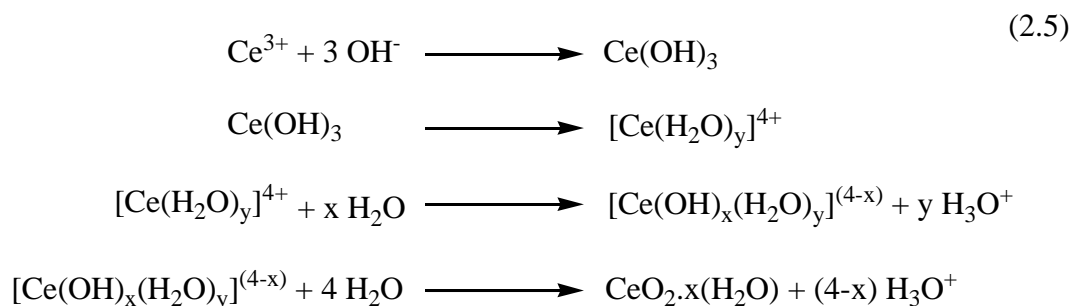
The graft density values of particles vary from 0.9 to 4.1 molecules/nm² for in situ approach. When the size of surfactant molecule is compared with the graft density, it is observed that there is an inverse relation between each other. The smaller the surfactant molecule, the higher the graft density is. Hence, the graft density is the highest in TGA functionalization. On the other hand, graft density of CTAB is the lowest one due to having the largest size. Nevertheless, the graft density lies in the range of 0.1 to 3.9 molecules/nm² for ex situ approach. The differences in graft density

values of two approaches suggest that denser surface functionalization is obtained by in situ approach compared to ex situ approach.

2.2.4. The Mechanism of Particle Formation

The molecules and extended solids those contain bonds between a transition metal ion and one or more ligands are called as coordination compounds (or complexes). In these coordinate covalent bonds, the metal ions and the ligands act as Lewis acids and Lewis bases, respectively. The bond is formed by overlap of the molecular orbital containing the lone pair electron of the ligand with the d-orbitals of the metal ion. Ligands in coordination complexes can be neutral molecules (H₂O, NH₃, organic bases such as pyridine, CO, NO, H₂, ethylene, and phosphines PR₃) and anions (halides, CN⁻, SCN⁻, cyclopentadienide (C₅H₅⁻), H⁻, etc.). The resulting complexes can be cationic, neutral, or anionic (<http://en.wikibooks.org/>).

The mechanism of particle formation is given in equation (2.5). At room temperature, the reaction of cerium (III) nitrate with ammonia forms the precipitate gelatinous hydrous cerium (IV) oxide (Lin and Chowdhury 2010). Precipitation of Ce(OH)₃ is observed due to the low solubility constant of this compound ($K_{sp} = 7 \times 10^{-21}$) as soon as ammonia is added to a cerium (III) precursor solution (Zhou et al. 2002). Ce(OH)₃ is oxidized to hydrated Ce(IV) ions in alkaline environment (Djuricic and Pickering 1999), and hydrolyzed to form complex [Ce(OH)_x(H₂O)_y]^{(4-x)+} (Hirano and Kato 1999, Chen and Chen 1993). Finally, water molecules deprotonate the complex (Djuricic and Pickering 1999, Chen and Chang, 2005) and the nucleation of ceria nanoparticles occur. The hydroxyl ion content in the process strongly affects the supersaturation degree of the initial precipitate and the oxidation of Ce(III) to Ce(IV) (Zhou et al. 2002, Chen and Chen 1993).



The growth of CeO₂ nanocrystals can be investigated by the intensity ratio of (111) and (200) crystallite planes in XRD patterns. This simple ratio may give some hints about the particle morphology and the results of both in situ and ex situ functionalized particles are given in Table 2.8.

Table 2.8. Comparison of the intensity ratio of (111) and (200) reflections in XRD patterns

particle	(111)/(200) intensity ratio	
	in situ	ex situ
unfunctionalized ceria	2.95	3.78
ceria(-MPS)	1.43	3.80
ceria(-CTAB)	1.74	3.86
ceria(-MPA)	1.47	3.87
ceria(-TGA)	1.49	3.86

In the crystallization of CeO₂, the crystal morphology changes from truncated octahedral to cuboctahedral, then further cubic structure. In the absence of surfactants, the (111) plane grows slower than the (200) one. Hence, the nanocrystals demonstrate cuboctahedral morphology. This ratio is decreased from 2.95 in the unfunctionalized particles to approximately 1.50 in the surface-functionalized ones for in situ functionalization. Based on the intensity ratio values, the particles demonstrate cubic morphology in the presence of surfactant molecules regardless of the type of surfactant. The surfactant molecules prefer (200) planes to adsorb and slow down the growth of these planes. Thus, the growth of (111) planes fasten and well defined cubic morphology is obtained. On the other hand, there is no any remarkable change in the

intensity ratio values between unfunctionalized and functionalized particles in ex situ approach. This result shows that surfactant molecules are not adsorbed by (200) plane and have no remarkable effect on ex situ functionalization. All particles possess truncated octahedral in ex situ approach.

CHAPTER 3

EFFECT OF SURFACE FUNCTIONALIZED CeO₂ NANOPARTICLES IN FREE RADICAL BULK POLYMERIZATION OF METHYL METHACRYLATE

3.1. Experimental

3.1.1. Materials and Methods

A sample of 30 mg powder was dispersed into 1 mL of MMA. The dispersions were sonicated in an ultrasonic bath for 30 min. In order to achieve complete wetting of the particle surface, the dispersions were kept overnight at room temperature. Benzoyl peroxide, BPO, (1.5 wt%) was added to the dispersion after a second ultrasonication for 30 min. Prior to polymerization, three cycles of a freeze-thaw process were utilized. Polymerization was performed at 60 °C and stopped after desired times (15, 30, 60, 120, 180, 240, 300, and 1020 min) by quenching to room temperature.

3.1.2. Characterization

Conversion of MMA to PMMA was determined gravimetrically. Initial weight of polymerization reactor involving test tube, monomer, initiator, and ceria nanoparticles is subtracted from final weight of the reaction system after complete removal of residual monomer under vacuum. Molecular weight distributions were determined by size exclusion chromatography (SEC). Both the polymers and composites were dissolved by toluene. After centrifugation at 6000 rpm, the nanoparticles were removed from polymer solution. Then, the remaining polymer solution was poured into excess methanol in order to precipitate the polymer. Finally, this precipitated polymer was used for SEC analysis. AFM measurements were

performed by Nanoscope IV Digital Instruments-MMSPM instrument in tapping mode in tapping mode scanning 5×5 , 3×3 , and $1\times 1\ \mu\text{m}^2$ area, respectively.

3.2. Results and Discussion

3.2.1. In -situ Polymerization of CeO₂/MMA Dispersion

Both in situ and ex situ functionalized CeO₂ particles were dispersed in MMA monomer where the weight fraction of particles were kept at 0.03 with respect to MMA in dispersion. The dispersions were exposed to bulk polymerization initiated by benzoyl peroxide (BPO) at 60 °C. The rate of polymerization, molecular weight (MW), and molecular weight distribution (MWD) were investigated separately for neat MMA, MMA in the presence of only capping agents, MMA dispersion containing unfunctionalized, in situ functionalized, and ex situ functionalized ceria particles.

3.2.2. Conversion

The polymerization is carried out at 80 °C at the initial state of the experiments and conversion of MMA in presence of both in situ and ex situ functionalized particles at this temperature is demonstrated in Figure 3.1. The decomposition half life of the initiator benzoyl peroxide (BPO) is 1.4 hours at 85 °C (Odián G. 2004). Since the decomposition is fast enough at this temperature, the complete conversion is enabled in a short time period. Hence, in order to observe the significant effect of particles on polymerization, the temperature is reduced to 60 °C where the decomposition half life of BPO is 100 hours (Bartlett and Hiatt 1958).

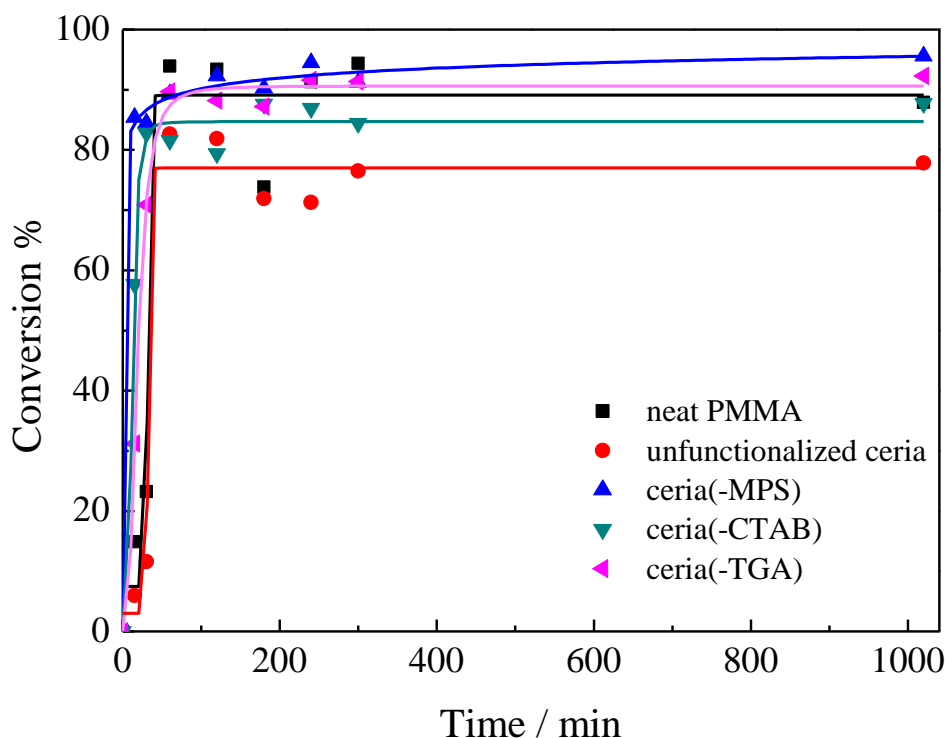


Figure 3.1. Conversion of MMA in presence of in situ functionalized CeO₂ nanoparticles at 80 °C.

Since the effects of particles on the polymerization has lost their significance, the temperature therefore was reduced to 60 °C, where $t_{1/2}=100$ h (Bartlett and Hiatt 1958). The conversion of MMA only (reference system) as a function of polymerization time is presented in Figure 3.2.a with dashed line. Not surprisingly, a sigmoidal increase with respect to time was obtained in the conversion curve most probably due to gel or Trommsdorf-Norrish effect. In free radical polymerization of vinyl monomers, the gel effect is commonly observed. Termination of a propagating radical is diffusion-controlled. As MMA is polymerized, the viscosity of the medium increases and the medium is then saturated with the amount of propagating radicals. The rate of termination dramatically decreases. Exothermic nature of addition polymerization triggers the propagation step; hence, autoacceleration of polymerization inevitably takes place. However, in the presence of particles (both unfunctionalized- and functionalized-CeO₂), the autoacceleration appears at longer time (Tunusoğlu and Demir 2013). Particles of hard solid spheres in polymerization medium may increase the viscosity of the polymerization mixture and hinder the diffusion of the radical chains so that polymerization is retarded by the particles regardless of the capping agents employed.

Moreover, lower conversion was observed in nanocomposite formation compared to the reference system. This result suggests that in situ functionalized particles showed inhibition for the polymerization. However, the presence of ex-situ functionalized ceria particles has no remarkable effect on the polymerization process (Figure 3.2.b). The reason of this result might be due to the loose and scarce grafting of the capping agents onto the particle surface.

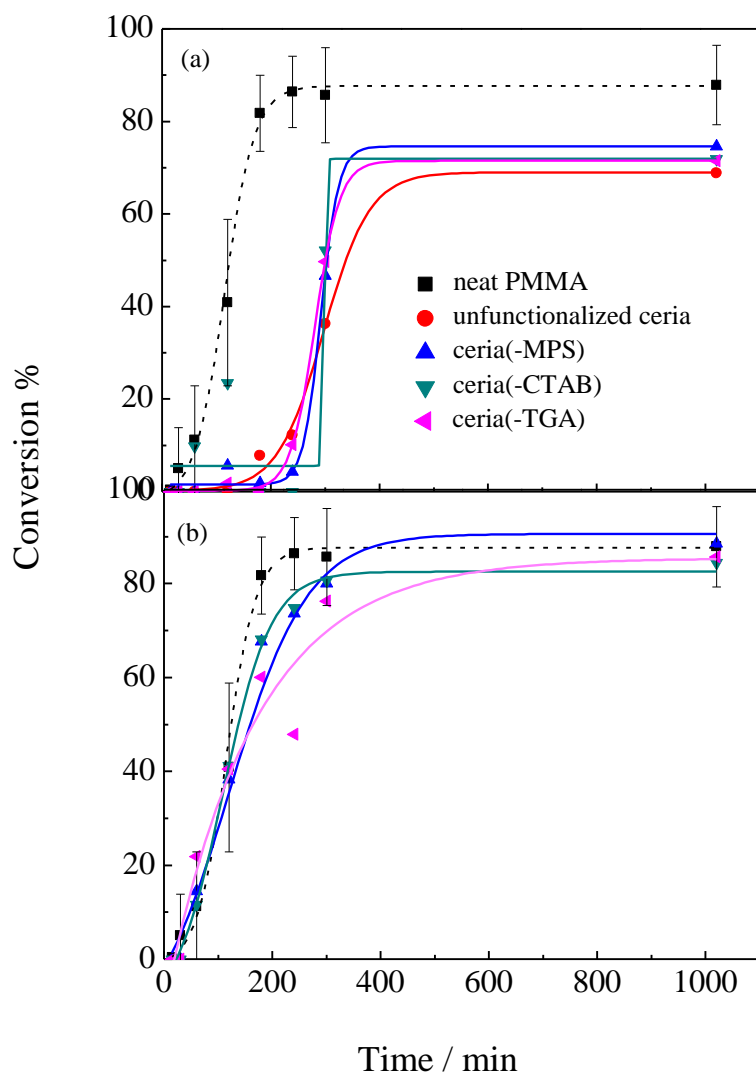


Figure 3.2. Conversion of MMA in the presence of (a) in situ and (b) ex situ functionalized CeO_2 nanoparticles at 60 °C.

3.2.3. Molecular Weight and Molecular Weight Distributions (MWD)

MWDs of PMMA synthesized in the presence of unfunctionalized and functionalized particles (both in situ and ex situ) is demonstrated in Figure 3.3.

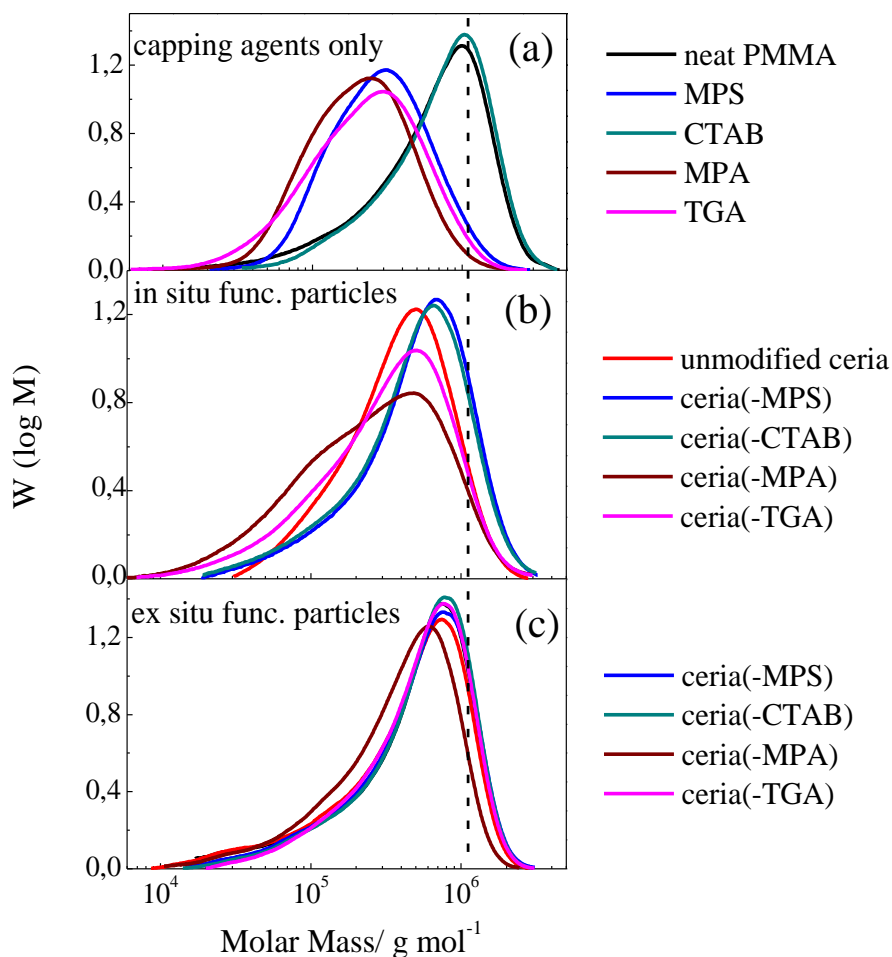


Figure 3.3. Molecular weight distribution of PMMA in presence of (a) cerium oxide functionalized in situ, (b) capping agents, and (c) ex situ over 1020 min of polymerization at 60 °C.

The same polymerization was carried out in the presence of neat capping agents only without the ceria particles. In addition, Table 3.1 gives number average molecular weight (M_n) and polydispersity index (PDI) of the MWDs given in Figure 3.3.

Table 3.1. Number molecular weight (M_n) and polydispersity index (PDI) of PMMA in the presence of neat capping agents, and cerium oxide functionalized in situ and ex situ over 1020 min of polymerization at 60 °C.

capping agent			in situ			ex situ		
sample	$M_n/\text{g mol}^{-1}$ ($\times 10^5$)	PDI (M_w/M_n)	sample	$M_n/\text{g mol}^{-1}$ ($\times 10^5$)	PDI (M_w/M_n)	sample	$M_n/\text{g mol}^{-1}$ ($\times 10^5$)	PDI (M_w/M_n)
neat PMMA	2.2	3.0	unfunctionalized ceria	2.6	1.9			
MPS	2.1	1.7	ceria(-MPS)	2.9	2.2	ceria(-MPS)	2.8	2.3
CTAB	4.6	1.9	ceria(-CTAB)	2.7	2.3	ceria(-CTAB)	2.9	2.3
MPA	1.5	1.8	ceria(-MPA)	1.3	3.0	ceria(-MPA)	2.1	2.3
TGA	1.4	2.2	ceria(-TGA)	1.6	2.9	ceria(-TGA)	3.1	2.1

3.2.3.1. Capping Agents Only without the Ceria Particles

Panel a of Figure 3.3 shows MWDs of PMMA obtained in the presence of capping agents as well as reference PMMA (MMA only). PMMA obtained from the reference system has a wide bimodal distribution and the MW appears to be very high at $2.2 \times 10^5 \text{ g mol}^{-1}$. It is well-known that bulk polymerization is an uncontrolled way of polymerization such that chain population is not uniform and composed of both small and large chains. PMMA obtained in the presence of CTAB has a higher MW ($4.6 \times 10^5 \text{ g mol}^{-1}$). Ghosh and Maity proposed a complexation taking place between BPO and CTAB in the free-radical polymerization of MMA (Gosh and Maity 1978). This complexation involves Coulombic interaction of BPO and cationic end of CTAB that causes bond breakage between oxygen atoms of peroxide. The complexation mechanism between BPO and CTAB is demonstrated in Figure 3.4 and given in Equation (3.1).

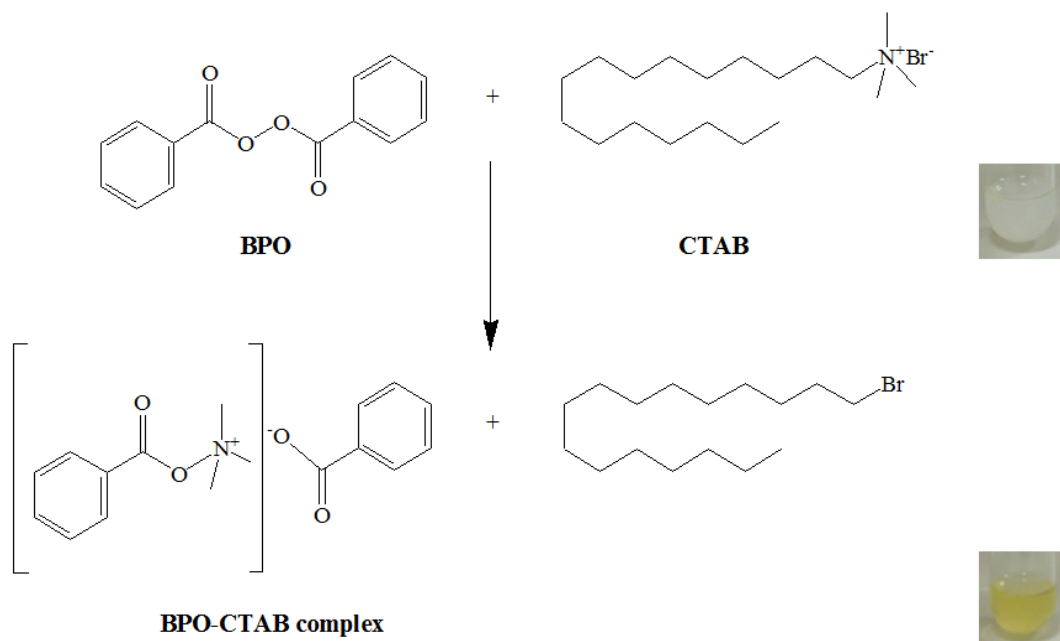
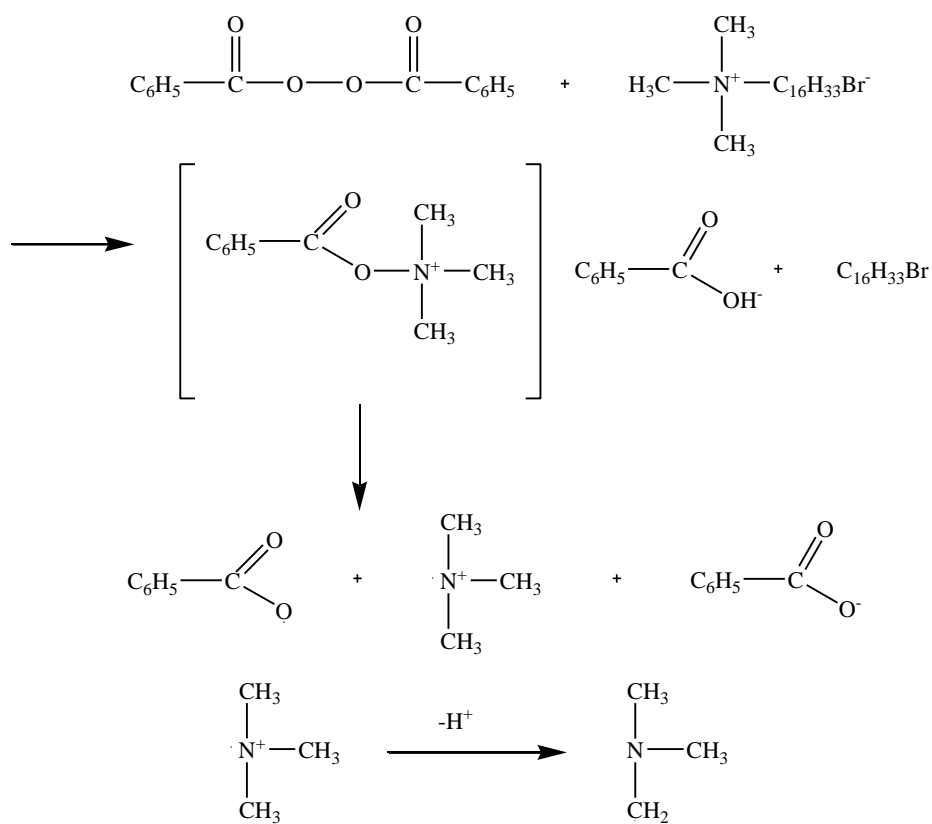


Figure 3.4. The reaction mechanism between CTAB and BPO

(3.1)



Ghosh and Maity (Ghosh and Maity 1978) state that although initiation of polymerization proceeds through amine radicals, it might be possible to provide the initiation of vinyl polymers with bromine or bromine complexes as initiators. The resulting cationic group behaves itself as a radical by leaving the complex. The colorless polymerization mixture turned into yellow upon this complexation. As a result, the efficiency of BPO was reduced so that higher MW chains are obtained. On the other hand, the PMMA chains obtained in the presence of thiol-containing agents appear to have lower molecular weight. The molecular weight of PMMA chains obtained in the presence of TGA, MPA, and MPS was 1.4×10^5 , 1.5×10^5 , and $2.1 \times 10^5 \text{ g mol}^{-1}$, respectively. It is well established that classical transfer agents reduce the molecular weight. Thiols have been recognized as chain transfer agents. The reactivity of a propagating radical is transferred to the sulfur atom. The sulfur radical is stable, and further propagation with a fresh monomer is not favorable (Bartlett and Hiatt 1958, Murray et al. 1999, Odian 2004). Since small molecules diffuse faster in polymerization, the function of the thiol in such molecules appears to be more efficient. Thus, the smaller the molecule is, the lower the MW.

3.2.3.2. Unfunctionalized Particles

For PMMA composites prepared with unfunctionalized particles, M_n was found to be $2.6 \times 10^5 \text{ g mol}^{-1}$. This MW is higher than that of the reference PMMA. Vibrational spectroscopy confirmed the interaction between BPO and ceria particle surface. Figure 3.5 presents the FTIR spectra of unfunctionalized particles, BPO itself, and unfunctionalized particles treated with BPO at 60 °C.

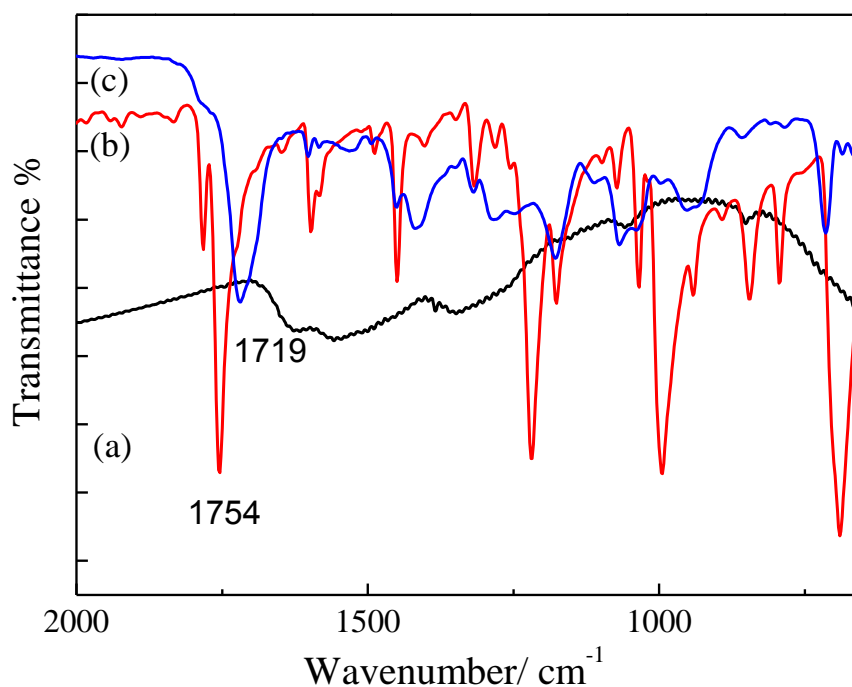


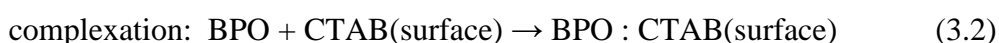
Figure 3.5. FTIR spectra of (a) unfunctionalized CeO_2 , (b) BPO, and (c) CeO_2 -BPO particles.

The unfunctionalized particles have weak and broad signals, i.e., do not have specific feature in this segment of the spectrum. On the other hand, BPO shows characteristic sharp vibrational signals. The fingerprint signals of BPO were found to be broadened and significantly shifted in BPO-treated ceria particles. For example, the stretching of the $\text{C}=\text{O}$ group of BPO is shifted from 1754 to 1719 cm^{-1} and full width half-maximum of this signal is broadened $\sim 15 \text{ cm}^{-1}$. The change in this spectral signal indicates the occurrence of a strong interaction of BPO with the ceria particle surface such that the efficiency of the initiator decreases. Thus, the chains synthesized in the presence of functionalized particles appear heavier than the reference PMMA.

3.2.3.3. In Situ Functionalized Particles

Panels b and c of Figure 3.3 show the MWDs of polymer obtained when in situ and ex situ shown passing through the mean of the distribution of PMMA (reference system). The critical micellar concentration (CMC) of CTAB is in the order of 10^{-3} M ;

therefore, the amount of CTAB used cannot exceed its CMC value. In the case of ceria(-CTAB), M_n is $2.7 \times 10^5 \text{ g mol}^{-1}$. The chains are heavier than the reference PMMA and lighter than the chains obtained in the presence of free CTAB. This result suggests that CTAB is still active in the aforementioned complexation with BPO when it is immobilized to the particle surface; so that, higher molecular weight than the reference PMMA was obtained. On the other hand, its function remarkably decreases compared to the one obtained in the presence of free CTAB without ceria particles most probably due to steric hindrance. As a result, molecular weight appears to be lighter.



The use of thiol-capped particles yields PMMA chains that have a lower MW than that of the reference. The surface thiol groups are usual suspect for the decrease in MW. The propagating MMA radical is transferred to particle surface and further propagation is prevented.



However, the function of the thiol-capped particles in polymerization is varied and is somewhat different from their role when they are free in the monomer without particles. For example, although TGA was the most effective transfer agent used in this study due to its smaller size, ceria(-MPA) as a chain transfer agent functions more effectively than ceria(-TGA). Both MPA and TGA have a similar structure as well as similar grafting to the particle surface via carboxylic acid. In contrast to TGA, MPA has CH_2 as its spacer group. When they are immobilized to the particle surface, ceria(-MPA) provides better mobility and flexibility for the thiol end-group and correspondingly better function in the transfer reaction. Another example for the variation of the role of the capping agents in polymerization when they are immobilized to the particle surface could be the role of ceria(-MPS). Surprisingly, it has almost no chain transfer function. Thiol is a good nucleophile, and it has tendency to attack silane groups in the molecule. In fact, the thiol group particularly becomes even more nucleophilic in a basic medium, which is the case for the particle synthesis where NH_4OH is a precursor. MPS molecules on the particle surface undergo self-

condensation between the silane and thiol groups (Jacobine 1993) and methanol is eliminated as a result of condensation. Thiol is, therefore, blocked by silane, and the function of MPS as a transfer agent is suppressed.

3.2.3.4. Ex Situ Functionalized Particles

M_n of PMMA obtained in the presence of ex situ functionalized particles was found in between 2.1 and $3.1 \times 10^5 \text{ g mol}^{-1}$. This range is relatively narrow compared to the chains produced in the presence of in situ functionalized particles ($1.3\text{--}2.9 \times 10^5 \text{ g mol}^{-1}$). Therefore, the ex situ functionalized particles are not as effective as the in situ functionalized ones in the development of molecular weight. A similar result was also obtained for the conversion data (Figure 3.2). While in situ functionalized particles cause retardation and inhibition in conversion, the ex situ functionalized particles did not have a remarkable effect on conversion. Yet, FTIR revealed the adsorption of the capping agents on the particles, and TGA confirmed the presence of the capping agents on the particle surface. The reason for the inertness of the ex situ functionalized particle in the polymerization process may lie on the surface feature, i.e., the process of functionalization. While monolayer coverage of the capping agents can be achieved for the in situ functionalized particles, similar homogeneity cannot be obtained for the ex situ functionalized ones. In the process, the surface functionalization is carried out for the isolated and redispersed particles; therefore, the particles remain as aggregated and functionalization takes place for the large aggregated particle domains instead of functionalization of the single individual particles. Moreover, the capping agent molecules may not be distributed evenly throughout the surface of ex situ functionalized particles; rather, clusters of the capping agents may be adsorbed to the particles surface sparsely. Thus, the heterogeneous surface functionalization passivate neat ceria surface, however, does not contribute to the free radical polymerization.

3.2.4. Level of Nanoparticle Dispersion in PMMA

The dispersibility of particles in a polymer matrix is a key point in polymer nanocomposites. AFM was employed for the determination of the dispersibility of the particle domains. Table 3.2 shows the average diameter of particle domains measured by tapping mode AFM images.

Table 3.2. Particle domain size in PMMA based on the statistical treatment of particles domains in tapping mode AFM phase images.

Ceria particles used in the composites	particle domain size in PMMA (nm)	
	in situ	ex situ
unfunctionalized ceria	27±4	25±9
ceria(-MPS)	48±12	61±10
ceria(-CTAB)	21±6	21±4
ceria(-TGA)	21±3	29±6

A representative set of the phase image of nanocomposites containing both in situ and ex situ functionalized ceria(-TGA) particles at 3 wt % is demonstrated in Figure 3.6.

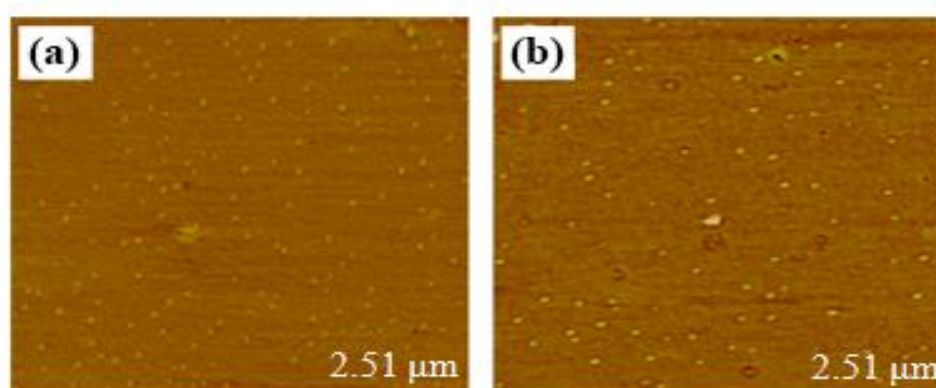


Figure 3.6. AFM images of in situ (a) and ex situ (b) TGA functionalized CeO₂ nanoparticles.

In comparison to the particle size in MMA based on DLS results given in Table 2.6, the domain size of both types of particles in PMMA appears to be smaller. Independent of the surface chemistry and approach employed in surface functionalization, the particles showed good dispersion in the polymer matrix. The domain size is <50 nm, which is 1 order of magnitude smaller than their size in MMA. We think that the smaller domain size in the polymer might be the result of subsequent freeze–thaw processes we applied three times prior to in situ polymerization. The colloidal destabilization of latexes by freezing is investigated by Blackley. It is stated that the freezing process begins with the reduction of temperature leading to the appearance of a third phase: pure ice. The polymer particle concentration in unfrozen water and the frequency of encounters between particles were increased by the formation of ice crystals. Under the high pressures from growing ice crystals, the polymer particles are forced into contact with each other which results in particle aggregation and interparticle coalescence. In the case of freeze and thaw instability with polymer latex, it has not been possible to conclude whether coagulation takes place during freezing or during thawing. For this reason, freeze-thaw stability covers both the freezing and thawing processes (www.thefreelibrary.com). Quenching the particle/MMA dispersion to very low temperature (to the temperature of liquid nitrogen) and subsequent heating to RT causes a serious volumetric change. Even if the nanosized particles contribute to the formation of aggregates/agglomerates, they were eventually deagglomerated by the end of this freeze and thaw process.

3.2.5. Thermal Properties of Nanocomposites

Degradation profiles of the PMMA composites in air and the derivative of thermal degradation (DTG) of both neat PMMA and PMMA/CeO₂ composites prepared by in situ functionalized nanoparticles obtained based on these profiles are given in Figure 3.7.

Three discrete degradation steps were clearly observed in the thermogram at around 160, 280, and 370 °C. This result agrees perfectly with the literature of the decomposition of PMMA (Demir et al. 2007, Kashiwagi et al. 2003). It is well established that the mechanism of radical termination in polymerization process has

strong influence on the thermal properties of the resulting composite material. There are two termination mechanisms: (i) combination and (ii) disproportionation (O'dian 2004). Both reactions yield abnormal linkages. The former one gives head-to-head linkages; in fact head-to-tail is the normal type of bonding for monomeric units. The latter one presents vinylidene end chains that unzip the chain under degradation conditions. These first two mass losses correspond to the decomposition of the head-to-head linkage and the unzipping of the vinylidene chain end, respectively. The main mass loss occurs around 370 °C due to the random chain scission. The intensity of this signal decreases for the chains obtained in the presence of ceria nanoparticles (both unfunctionalized and functionalized ones) and may be correlated with the molecular weight of the in situ formed PMMA chains. For example, when thiol capped ceria particles are used, the intensity of the signal decreases. The degradation of lower molecular weight chains readily occurs so that the intensity of the mass loss at 370 °C increases as the molecular weight decreases.

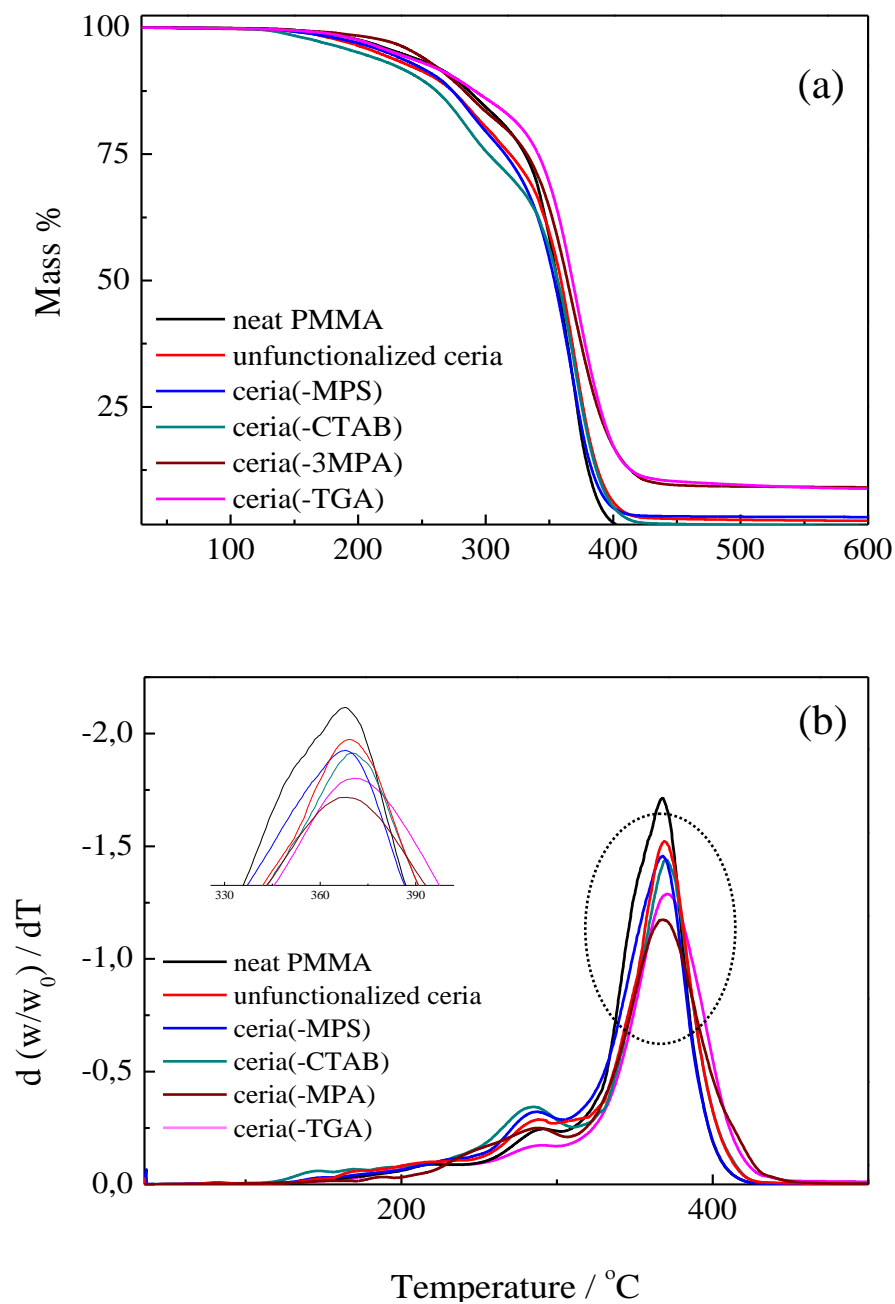


Figure 3.7. (a) TGA demonstration of neat PMMA and its composites and (b) DTG curves of thermal decomposition of neat PMMA and its composites prepared by both unfunctionalized and functionalized CeO_2 nanoparticles at 60 °C.

Interfacial attraction between particles and the surrounding PMMA matrix has significant influence on many macroscopic properties for instance glass transition temperature (T_g) of the polymer composites. The presence of the nanoparticles might

demonstrate either attractive or repulsive interaction; thus, a change in T_g is an evidence of these interactions. DSC can provide information about the comparative interaction of the particles functionalized either in situ or ex situ with the surrounding polymer matrix. When this interaction is attractive, polymer chains those are directly in contact with nanoparticles are decelerated and an increase in T_g occurs (Jancar et al. 2010). DSC curve and the value of each composite were given in Figure 3.8 and Table 3.3.

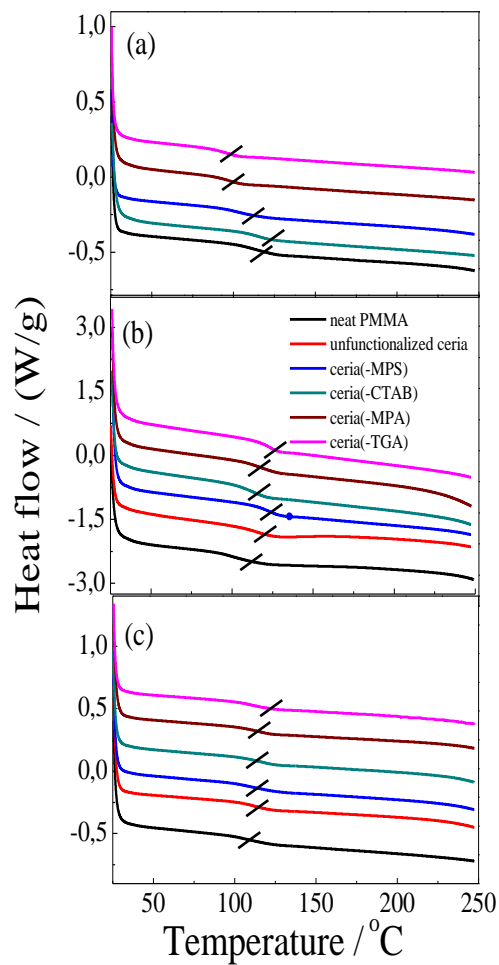


Figure 3.8. Glass transition temperature (T_g / °C) of PMMA in presence of (a) capping agents, and cerium oxide functionalized in situ (b) and ex situ (c) at 60 °C.

Table 3.3. Glass transition temperatures (T_g/°C) of PMMA prepared in the presence of capping agents, ceria nanoparticles surface functionalized both in situ and ex situ approaches at 60 °C

sample	PMMA with capping agent	sample	PMMA with in situ functionalized ceria	PMMA with ex situ functionalized ceria
MPS	103	ceria(-MPS)	123	111
CTAB	115	ceria(-CTAB)	114	117
MPA	98	ceria(-MPA)	117	116
TGA	96	ceria(-TGA)	123	113

The effects of neat surfactants on T_g of the polymer were given in the second column of Table 3.3. While T_g of neat PMMA was 108 °C, this temperature decreased to 103, 98, and 96 °C in the presence of capping agents MPS, MPA, and TGA. The addition of free capping agents without grafting to ceria nanoparticles decreases the T_g value. The capping agents are smaller molecules compared to PMMA chains and they act as a plasticizer that may reduce T_g. The glass transition temperature is increased to 116 °C when PMMA is prepared in the presence of unfunctionalized particles most probably due to the interaction between surface hydroxyls and the acrylate group of the PMMA chains. Similarly, a remarkable enhancement in the T_g value was observed by the addition of particles regardless of the surface feature (column four and five of Table 3.3). An increase in T_g can be the consequence of interactions between free functional –SH groups of the capping agents and carbonyl group of PMMA chains. In contrast, there is no any remarkable change between T_g of the polymer chains synthesized by the presence of neat CTAB and CTAB functionalized CeO₂ nanoparticles. The plasticizing effect of aliphatic chains-C18 may offset the increase of T_g due to the presence of nanoparticles. The composites prepared by ex situ functionalized particles do not show strong variation in T_g and lie between 111 and 117 °C, considering the T_g of composites prepared by unfunctionalized particles is 116 °C. One can conclude that the interaction of the ex situ functionalized particles and surrounding PMMA chains is

lower compared to the interaction with in situ functionalized ones with the PMMA matrix.

CHAPTER 4

CONCLUSIONS AND RECOMMENDATIONS

Controlled chemical precipitation of homogeneous CeO₂ nanoparticles of average size smaller than 10 nm with various surface functionalities was presented. The most significant aspect of our synthesis method is that almost any functionality can be introduced onto the surfaces of nanoparticles by choosing appropriate molecules as capping ligands. Although only thiol, aliphatic, and carboxylic groups are chosen here to demonstrate the idea, molecules with other functional groups such as aldehyde, epoxide, amine can also be used as the capping agents to build a specific ligand shell. The compatibility of the resulting particles with MMA demonstrated that the procedure can be developed into a general one for the preparation of ceria nanoparticles with versatile surface functionalities. This simple approach is promising for future large-scale synthesis of this nanostructured material for many important applications in catalysis, optoelectronics, and oxygen storage capacity medium in a controlled manner.

PMMA composites including ceria nanoparticles were prepared by free radical in situ bulk polymerization using BPO as initiator. Surface functionalization of the CeO₂ nanoparticles was carried out using various surfactant molecules having different chemistry (TGA, MPA, MPS, and CTAB) employing both in situ and ex situ approaches. We have shown that how the particle surface functionalization is performed plays a decisive role in the polymerization process. While in situ functionalized CeO₂ nanoparticles contributed to polymerization, the influences of ex situ functionalized ones were not noteworthy although the same surfactant molecules were used with the same amount. For example, in situ functionalized particles cause retardation and inhibition in the polymerization; however, a remarkable influence was not observed when ex situ functionalized particles were employed. The result is presumably due to the fact that the in situ approach provides densely and homogeneously covered the particle surface. The freeze and thaw process was found to be useful in the process of in situ polymerization. It causes severe deagglomeration, even for the unfunctionalized particles that strongly contribute to aggregation/agglomeration in MMA. A systematic study focusing on the effect of the substrate (silica, zincite, and titania), level of particle

loading, polymerization temperature, and type of free-radical initiator may shed light on the detailed mechanism of the process of in situ polymerization. For further studies, the variation of surface capping agents on particle surfaces can be investigated in order to observe the effects of the surface chemistry on conversion and molecular weight distributions of polymers synthesized by in situ method.

REFERENCES

- Ahmadi, S. J., Huang, Y. D., and Li, W. 2004. Synthetic routes, properties and future applications of polymer-layered silicate nanocomposites. *Journal of Materials Science* 39 (6): 1919-1925.
- Akbey, U., Franks, W. T., Linden, A., Lange, S., Griffin, R. G., van Rossum, B. J., and Oschkinat, H. 2010. Dynamic nuclear polarization of deuterated proteins. *Angewandte Chemie International Edition* 49 (42): 7803–7806.
- Anžlovar, A., Orel, Z. C., and Žigon, M. 2010. Poly(methyl methacrylate) composites prepared by in situ polymerization using organophilic nano-to-submicrometer zinc oxide particles. *European Polymer Journal* 46 (6): 1216-1224.
- Baniasadi, H., Ramazani, A., and Nikkhah, S. J. 2010. Investigation of in situ prepared polypropylene/clay nanocomposites properties and comparing to melt blending method. *Materials & Design* 31 (1): 76-84.
- Bartlett, P. D., and Hiatt, R. R. A. 1958. Series of tertiary butyl peresters showing concerted decomposition. *Journal of the American Chemical Society* 80 (6): 1398-1405.
- Campos, C. L., Roldán, C., Aponte, M., Ishikawa, Y., and Cabrera, C. R. 2005. Preparation and methanol oxidation catalysis of Pt-CeO₂ electrode *Journal of Electroanalytical Chemistry* 581 (2): 206-215.
- Chang, C. C., Chen, P. H., and Chang, C. M. 2008. Preparation and characterization of acrylic polymer-nanogold nanocomposites from 3-mercaptopropyltrimethoxysilane encapsulated gold nanoparticles. *Journal of Sol-Gel Science and Technology* 47 (3): 268–273.
- Chen, P. L., Chen, I. W. 1993. Reactive cerium (IV) oxide powders by the homogeneous precipitation method. *Journal of American Chemical Society* 76 (6): 1577-1583.
- Chen, H. I., and Chang, H. Y. 2005. Synthesis of nanocrystalline cerium oxide particles by the precipitation method. *Ceramics International* 31 (6): 795–802.
- Chen, P. L., and Chen, I. W. 1993. Reactive cerium (IV) oxide powders by the homogeneous precipitation method. *Journal of the American Ceramic Society* 76 (6): 1577–1583.
- Corma, A., Atienzar, P., Garcia, H., and Chane-Ching, J. Y. 2004. Hierarchically mesostructured doped CeO₂ with potential for solar-cell use. *Nature Materials* 3 (6): 394–397.
- Demir, M. M., Soyak, D., Unlu, C., Kus, M., and Ozcelik, S. 2009. Controlling spontaneous emission of CdSe nanoparticles dispersed in electrospun fibers of

- polycarbonate urethane. *The Journal of Physical Chemistry C* 113 (26): 11273–11278.
- Demir, M. M., Muñoz-Espí, R., Lieberwirth, I., and Wegner, G. 2006. Precipitation of monodisperse ZnO nanocrystals via acid-catalyzed esterification of zinc acetate. *Journal of Materials Chemistry* 16 (28): 2940–2947.
- Demir, M. M., Koynov, K., Akbey, U., Bubeck, C., Park, I., Lieberwirth, I., and Wegner, G. 2007. Optical properties of composites of PMMA and surface-modified zincite nanoparticles. *Macromolecules* 40 (4): 1089–1100.
- Demir, M. M., Castignolles, P., Akbey, U., and Wegner, G. 2007. In situ bulk polymerization of dilute particle/MMA dispersions. *Macromolecules* 40 (12): 4190-4198.
- Demir, M. M., and Wegner, G. 2012. Challenges in the preparation of optical polymer composites with nanosized pigment particles: a review on recent efforts. *Macromolecular Materials and Engineering* 297 (9): 838-863.
- Demir, M. M., Memesa, M., Castignolles, P., and Wegner, G. 2006. PMMA/Zinc oxide nanocomposites prepared by in situ bulk polymerization. *Macromolecular Rapid Communications* 27 (10): 763-770.
- Demir, M. M., Koynov, K., Akbey, U., Bubeck, C., Park, I., Lieberwirth, I., and Wegner, G. 2007. Optical properties of composites of PMMA and surface-modified zincite nanoparticles. *Macromolecules* 40 (4): 1089-1100.
- Dieckmann, Y., Cölfen, H., Hofmann, H., and Petri-Fink, A. 2009. Particle size distribution measurements of manganese-doped ZnS nanoparticles. *Analytical Chemistry* 81(10): 3889-3895.
- Djuricic, B., and Pickering, S. 1999. Nanostructured cerium oxide: preparation and properties of weakly-agglomerated powders. *Journal of the European Ceramic Society* 19 (11): 1925–1934.
- Ghosh, P., and Maity, S. N. 1978. Polymerization of methyl-methacrylate with use of acetyl trimethyl ammonium bromide benzoyl peroxide combination as initiating system. *European Polymer Journal* 14 (10): 855-859.
- Gorna, K., Muñoz-Espí, R., Gröhn, F., and Wegner, G. 2007. Bioinspired mineralization of inorganics from aqueous media controlled by synthetic polymers. *Macromolecular Bioscience* 7 (2): 163-173.
- Gorrasi, G., Tortora, M., Vittoria, V., Pollet, E., Lepoittevin, B., Alexandre, M., and Dubois, P. 2003. Vapor barrier properties of polycaprolactone montmorillonite nanocomposites: effect of clay dispersion. *Polymer* 44 (8): 2271-2279.
- Griffin, R.G. 2010. Spectroscopy clear signals from surfaces. *Nature* 468 (7322): 381–382.

- Hess, S., Demir, M. M., Yakutkin, V., Balushev, S., and Wegner, G 2009. Investigation of oxygen permeation through composites of PMMA and surface-modified ZnO nanoparticles. *Macromolecular Rapid Communications* 30 (4-5): 394-401.
- Hirano, M., and Kato, E. 1999. Hydrothermal synthesis of nanocrystalline cerium(IV) oxide powders. *Journal of the American Ceramic Society* 82 (3): 786–788.
- http://en.wikibooks.org/wiki/Introduction_to_Inorganic_Chemistry/Coordination_Chemistry_and_Crystal_Field_Theory#.C2.A0.C2.A05.3_Spectrochemical_series
- <http://www.thefreelibrary.com/Direct+observation+of+freeze-thaw+instability+of+latex+coatings+via...-a0145885062>
- Israelachvili, J. N. 2011. Intermolecular and surface forces. *Elsevier Netherlands*.
- Jacobine, A. F. Radiation Curing in Polymer Science and Technology, Elsevier: London, 1993.
- Jancar, J., Douglas, J. F., Starr, F. W., Kumar, S. K., Cassagnau, P., Lesser, A. J., Sternstein, S. S., and Buehler, M. J. 2010. Current issues in research on structure-property relationships in polymer nanocomposites. *Polymer* 51 (15): 3321-3343.
- Kashiwagi, T., Morgan, A. B., Antonucci, J. M., VanLandingham, M. R., Harris, R. H., Awad, W. H., and Shields, J. R. 2003. Thermal and flammability properties of a silica-poly-(methylmethacrylate) nanocomposite. *Journal of Applied Polymer Science* 89 (8): 2072-2078.
- Kepenekci, O., Emirdag-Eanes, M., and Demir, M. M. 2011. Effect of alkali metal hydroxides on the morphological development and optical properties of ceria nanocubes under hydrothermal conditions. *Journal of Nanoscience and Nanotechnology* 11 (4): 3565–3577.
- Lafon, O., Rosay, M., Aussenac, F., Lu, X.Y., Trebosc, J., Cristini, O., Kinowski, C., Touati, N., Vezin, H., and Amoureux, J.P. 2011. Beyond the silica surface by direct silicon-29 dynamic nuclear polarization. *Angewandte Chemie International Edition* 50 (36): 8367–8370.
- Larese, C., Granados M. L., Galisteo, F. C., Mariscal, R., and Fierro, J. L. G. 2006. TWC deactivation by lead: a study of the Rh/CeO₂ system. *Applied Catalysis B: Environmental* 62 (1-2): 132–143.
- Lawrence, N. J., Brewer, J. R., Wang, L., Wu, T. S., Wells-Kingsbury, J., Ihrig, M. M., Wang, G. H., Soo, Y. L., Mei, W. N., and Cheung, C. L. 2011. Defect engineering in cubic cerium oxide nanostructures for catalytic oxidation. *Nano Letters* 11 (7): 2666-2671.
- LeBaron, P. C., Wang, Z., and Pinnavaia, T. J. 1999. Polymer-layered silicate nanocomposites: an overview. *Applied Clay Science* 15 (1-2): 11-29.

- Lee, T. Y., and Bowman, C. N. 2006. The effect of functionalized nanoparticles on thiol-ene polymerization kinetics. *Polymer* 47 (17): 6057-6065.
- Lelli, M., Gajan, D., Lesage, A., Caporini, M. A., Vitzthum, V., Mieville, P., Heroguel, F., Rascon, F., Roussey, A., Thieuleux, C., Boualleg, M., Veyre, L., Bodenhausen, G., Coperet, C., and Emsley, L. 2011. Fast characterization of functionalized silica materials by silicon-29 surface-enhanced NMR spectroscopy using dynamic nuclear polarization. *Journal of the American Chemical Society* 133 (7): 2104–2107.
- Lesage, A., Lelli, M., Gajan, D., Caporini, M. A., Vitzthum, V., Mieville, P., Alauzun, J., Roussey, A., Thieuleux, C., Mehdi, A., Bodenhausen, G., Coperet, C., and Emsley, L. 2010. Surface enhanced NMR spectroscopy by dynamic nuclear polarization. *Journal of the American Chemical Society* 132 (44): 15459–15461.
- Lin, K. S., and Chowdhury, S. 2010. Synthesis, characterization, and application of 1-D cerium oxide nanomaterials: a review. *International Journal of Molecular Sciences* 11 (9): 3226–3251.
- Lin, Z., Cheng, Y. R., Lu, H., Zhang, L. A., and Yang, B. 2010. Preparation and characterization of novel ZnS/sulfur-containing polymer nanocomposite optical materials with high refractive and high nanophase contents. *Polymer* 51 (23): 5424-5431.
- Lu, X. W., Li, X. Z., Chen, F., Ni, C. Y., and Chen, Z. G. 2009. Hydrothermal synthesis of prism-like mesocrystal CeO₂. *Journal of Alloys and Compounds* 476 (1-2): 958–962.
- Maensiri, S., Masingboon, C., Laokul, P., Jareonboon, W., Promarak, V., Anderson, P. L., and Seraphin, S. 2007. Egg white synthesis and photoluminescence of platelike clusters of CeO₂ nanoparticles. *Crystal Growth & Design* 7 (5): 950–955.
- Maskell, W. C. 2000. Progress in the development of zirconia gas sensors. *Solid State Ionics* 134 (1-2): 43–50.
- Masui, T., Hirai, H., Hamada, R., Imanaka, N., Adachi, G., Sakata, T., and Mori, H. 2003. Synthesis and characterization of cerium oxide nanoparticles coated with turbostratic boron nitride. *Journal of Materials Chemistry* 13 (3): 622–627.
- Matolín, V., Matolínová, I., Sedláček, L., Prince, K.C., Skála, T. 2009. A resonant photoemission applied to cerium oxide based nanocrystals. *Nanotechnology* 20 (21).
- Moniruzzaman, M., and Winey, K. I. 2006. Polymer nanocomposites containing carbon nanotubes. *Macromolecules* 39 (16): 5194-5205.
- Muñoz-Espí, R., Qi, Y., Lieberwirth, I., Gomez, C. M., and Wegner, G. 2006. Surface functionalized latex particles as controlling agents for the mineralization of zinc oxide in aqueous medium. *Chemistry-A European Journal* 12 (1): 118–129.

- Murray, E. P., Tsai, T., and Barnett, S. A. 1999. A direct-methane fuel cell with a ceria-based anode. *Nature* 400 (6745): 649-651.
- Nazarenko, S., Meneghetti, P., Julmon, P., Olson, B. G., and Qutubuddin, S. 2007. Gas barrier of polystyrene montmorillonite clay nanocomposites: effect of mineral layer aggregation. *Journal of Polymer Science Part B: Polymer Physics* 45 (13): 1733-1753.
- Niesz K., Reji C., Neilson J.R., Vargas R.C., and Morse D.E. 2010. Unusual evolution of ceria nanocrystal morphologies promoted by a low-temperature vapor diffusion based process. *Crystal Growth & Design* 10 (10): 4485-4490.
- Odian, G. Principles of Polymerization, 4th ed. John Wiley & Sons, Inc., New York, 2004.
- Oh, H., and Kim, S. 2007. Synthesis of ceria nanoparticles by flame electrospray pyrolysis. *Journal of Aerosol Science* 38 (12): 1185-1196.
- Olad, A., and Rasouli, H. 2010. Enhanced corrosion protective coating based on conducting polyaniline/zinc nanocomposite. *Journal of Applied Polymer Science* 115 (4): 2221-2227.
- Orel, Z.C., and Orel, B. 1994. Optical-properties of pure CeO₂ and mixed CeO₂/SnO₂ thin film coatings. *Physica Status Solidi (b)* 186 (1): K33-K36.
- Palard, M., Balencie, J., Maguer, A., and Hochepped, J. F. 2010. Effect of hydrothermal ripening on the photoluminescence properties of pure and doped cerium oxide nanoparticles. *Materials Chemistry and Physics* 120 (1): 79-88.
- Parlak, O., and Demir, M. M. 2011. Toward transparent nanocomposites based on polystyrene matrix and PMMA-grafted CeO₂ nanoparticles. *ACS Applied Materials & Interfaces* 3 (11): 4306-4314.
- Saric, M., Dietsch, H., and Schurtenberger, P. 2006. In situ polymerisation as a route towards transparent nanocomposites: time-resolved light and neutron scattering experiments. *Colloids and Surfaces A-Physicochemical and Engineering Aspects* 291 (1-3): 110-116.
- Stevens, M. P. Polymer Chemistry: An Introduction; Oxford University Press, Inc.: New York, 1999.
- Sujana, M. G., Chattopadyay, K. K., and Anand, S. 2008. Characterization and optical properties of nano-ceria synthesized by surfactant-mediated precipitation technique in mixed solvent system. *Applied Surface Science* 254 (22): 7405-7409.
- Sun, C. W., Li, H., Zhang, H. R., Wang, Z. X., and Chen, L. Q. 2005. Controlled synthesis of CeO₂ nanorods by a solvothermal method. *Nanotechnology* 16 (9): 1454-1463.

- Taguchi, M., Takami, S., Naka, T., and Adschiri, T. 2009. Growth mechanism and surface chemical characteristics of dicarboxylic acid-modified CeO₂ nanocrystals produced in supercritical water: tailor-made water-soluble CeO₂ nanocrystals. *Crystal Growth & Design* 9 (12): 5297–5303.
- Taguchi, M., Takami, S., Adschiri, T., Nakane, T., Sato, K., and Naka, T. 2011. Supercritical hydrothermal synthesis of hydrophilic polymer-modified water-dispersible CeO₂ nanoparticles. *Crystal Engineering Communications* 13 (8): 2841–2848.
- Taniguchi, T., Watanabe, T., Sakamoto, N., Matsushita, N., and Yoshimura, M. 2008. Aqueous route to size-controlled and doped organophilic ceria nanocrystals. *Crystal Growth & Design* 8 (10): 3725–3730.
- Tjong, S. C. 2006. Structural and mechanical properties of polymer nanocomposites. *Materials Science and Engineering: R: Reports* 53 (3-4): 73-197.
- Tunusoğlu, Ö., Muñoz-Espí, R., Akbey, Ü., Demir, M. M. 2012. Surfactant-assisted formation of organophilic CeO₂ nanoparticles. *Colloids and Surfaces A: Physicochemical and Engineering Aspects* 395: 10-17.
- Tunusoğlu, Ö., Demir, M. M. 2013. Tailored CeO₂ nanoparticles surface in free radical bulk polymerization of methyl methacrylate. *Industrial & Engineering Chemistry Research* 52 (37): 13401–13410.
- Wang, C., Dong, B., Gao, G. Y., Xu, M. W., and Li, H. L. 2008. A study on microhardness and tribological behavior of carbon nanotubes reinforced AMMA-CNTs copolymer nanocomposites. *Materials Science and Engineering: A* 478 (1-2): 314-318.
- Wang, Z. L., and Feng, X. D. 2003. Polyhedral shapes of CeO₂ nanoparticles. *The Journal of Physical Chemistry B* 107 (49): 13563–13566.
- Wu, K. L., Chou, S. C., and Cheng, Y. Y. 2010. Comparison of polyimide/multiwalled carbon nanotube (MWNT) nanocomposites by in situ polymerization and blending. *Journal of Applied Polymer Science* 116 (6): 3111-3117.
- Wu, Z., Benfield, R.E., Guo, L., Li, H., Yang, Q., Grandjean, D., Li, Q., and Zhu, H. 2001. Cerium oxide nanoparticles coated by surfactant sodium bis(2-ethylhexyl) sulphosuccinate (AOT): local atomic structures and X-ray absorption spectroscopic studies. *Journal of Physics: Condensed Matter* 13 (22): 5269-5283.
- Yang, Z., Zhou, K., Liu, X., Tian, Q., Lu, D., and Yang, S. 2007. Single-crystalline ceria nanocubes: size-controlled synthesis, characterization and redox property. *Nanotechnology* 18 (18).
- Yu, S. H., Colfen, H., and Fischer, A. 2004. High quality CeO₂ nanocrystals stabilized by a double hydrophilic block copolymer. *Colloids Surfaces A: Physicochemical and Engineering Aspects* 243 (1-3): 49–52.

- Zhang, F., Chan, S.W., Spanier, J.E., Apak, E., Jin, Q., Robinson, R.D., and Herman, I.P. 2002. Cerium oxide nanoparticles: size-selective formation and structure analysis. *Applied Physics Letters* 80 (1): 127–129.
- Zhang, L., Li, F., Chen, Y. W., and Wang, X. F. 2011. Synthesis of transparent ZnO/PMMA nanocomposite films through free-radical copolymerization of asymmetric zinc methacrylate acetate and in situ thermal decomposition. *Journal of Luminescence* 131 (8): 1701-1706.
- Zhang, F., Jin, Q., Chan, S.W. 2004. Ceria nanoparticles: size, size distribution, and shape. *Journal of Applied Physics* 95 (8): 4319-4326.
- Zhang, F., Chan, S.W., Spanier, E.J., Apak, E., Jin, Q., Robinson, R.D., and Herman, I.P. 2002. Cerium oxide nanoparticles: size-selective formation and structure analysis. *Applied Physics Letters* 80 (1): 127-129.
- Zhang, Q.C., Yu, Z.H., Li, G., Ye, Q.M., and Lin, J.H. 2009. Synthesis of quantum-size cerium oxide nanocrystallites by a novel homogeneous precipitation method. *Journal of Alloys and Compounds* 477 (1-2): 81-84.
- Zhou, X. D., Huebner, W., and Anderson, H. U. 2002. Room-temperature homogeneous nucleation synthesis and thermal stability of nanometer single crystal CeO₂. *Applied Physics Letters* 80 (20): 3814–3816.
- Zhou, C. J., Qiu, X. Y., Zhuang, Q. X., Han, Z. W., and Wu, Q. L. 2012. In situ polymerization and photophysical properties of poly(p-phenylene benzobisoxazole)/ multiwalled carbon nanotubes composites. *Journal of Applied Polymer Science* 124 (6): 4740-4746.

VITA

PERSONAL INFORMATION

Surname, Name: TUNUSOĞLU ÖZGE
Nationality: Turkish (TC)
Date and Place of Birth: 23.07.1981, Bornova/İZMİR
Marital Status: Single
Phone: +90 (533) 445 56 91
E-mail: ozge_tunusoglu@yahoo.com



EDUCATION

Degree Institution Year of Graduation
MSc İzmir Institute of Technology 2007
BSc İzmir Institute of Technology 2004

WORK EXPERIENCE

Year Place Enrollment
2004-2013 İzmir Institute of Technology, Research Assistant
2013- now Ege Gümrük Ticaret Bölge Müdürlüğü, İzmir Laboratuvar Müdürlüğü

PUBLICATIONS

- Tunusoğlu, Ö., Muñoz-Espí, R., Akbey, Ü., Demir, M. M. 2012. Surfactant-assisted formation of organophilic CeO₂ nanoparticles. *Colloids and Surfaces A: Physicochemical and Engineering Aspects* 395: 10-17.
- Tunusoğlu, Ö., Demir, M. M. 2013. Tailored CeO₂ nanoparticles surface in free radical bulk polymerization of methyl methacrylate. *Industrial & Engineering Chemistry Research* 52 (37): 13401–13410.
- Tunusoğlu, Ö., Shahwan, T., Eroğlu, A. E. 2007. Retention of aqueous Ba²⁺ ions by calcite and aragonite over a wide range of concentrations: Characterization of the uptake capacity, and kinetics of sorption and precipitate formation. *Geochemical Journal* 41 (5): 379-389.
- Shahwan, T., Zünbul, B., Tunusoglu, O., Eroglu, A.E. 2005. AAS, XRPD, SEM/EDS, and FTIR characterization of Zn²⁺ retention by calcite, calcite-kaolinite, and calcite-clinoptilolite minerals. *Journal of Colloid and Interface Science* 286 (2): 471-478.